Titre: Title:	Stabilization of small metallic particles on functionalized pyrene
Auteur: Author:	Ramón Martínez
Date:	2008
Type:	Mémoire ou thèse / Dissertation or Thesis
Référence: Citation:	Martínez, R. (2008). Stabilization of small metallic particles on functionalized pyrene [Mémoire de maîtrise, École Polytechnique de Montréal]. PolyPublie. https://publications.polymtl.ca/8346/

UNIVERSITÉ DE MONTRÉAL

STABILIZATION OF SMALL METALLIC PARTICLES ON FUNCTIONALIZED PYRENE

RAMÓN MARTÍNEZ
DÉPARTEMENT DE GÉNIE PHYSIQUE
ÉCOLE POLYTECHNIQUE DE MONTRÉAL

MÉMOIRE PRÉSENTÉ EN VUE DE L'OBTENTION
DU DIPLÔME DE MAÎTRISE ÈS SCIENCES APPLIQUÉES
(GÉNIE PHYSIQUE)
AVRIL 2008

Your file Votre référence
ISBN: 978-0-494-46063-4
Our file Notre référence
ISBN: 978-0-494-46063-4

UNIVERSITÉ DE MONTRÉAL

ÉCOLE POLYTECHNIQUE DE MONTRÉAL

Ce mémoire intitulé:

STABILIZATION OF SMALL METALLIC PARTICLES ON FUNCTIONALIZED PYRENE

présenté par: MARTÍNEZ Ramón

en vue de l'obtention du diplôme de: Maîtrise ès sciences appliquées

a été dûment accepté par le jury d'examen constitué de:

M. DESJARDINS Patrick, Ph.D., président

M. ROCHEFORT Alain, Ph.D., membre et directeur de recherche

M. MASUT Remo A., Ph.D., membre

A mi amada llovizna de luna ...

ACKNOWLEDGEMENTS

I would like to give a million thanks to Alain Rochefort for giving me the opportunity to work here, in this country where ideas, instead of political ideologies, count. Alain, you have been more than a guiding hand, a friend, as a director you have granted me the freedom of expressing my own ideas, to work my own way. I will never able to pay you back for what you have done for myself and my family.

There is a family in Quèbec, that has become more than our family now: Nagy, Rosalba, Stephane & Jean-Luc Bedwani they opened their house and their hearts to us, like no one had before. Showing us what friendship is all about.

Thanks to a very good friend, who has been by my side during the good times and has lent me a helping hand during the hard ones. He is, also, the author of one of the most inspiring thought that I have encountered during my research:

> "Les nanotubes de carbone ont passé pendant longtemps inaperçu, probablement à cause de leur taille ..."

Thanks Stéphane for everything you have done for me and my family.

Thanks to my friend Louis-Phillippe (l'Otarien), he had the disgrace to read my manuscript first than anyone else. He corrected all from commas to tons of spanglishism. Thanks Louis, my family and I love you very much!

Thanks to our good friend Elyse Adam for your friendship and support, we love you! Ahh, yes there are "Castors" in Venezuela.

A million thanks to Gabriel Monett who trusted and helped me like a best friend

does.

To my very good friend Alexandre Beausoleil and his family, many thanks also.

Many thanks to Prof. Savadogo for open doors for me and my family.

Finally, a very special thanks to my dear friend Kostas Piyakis for allowing me to "kill" Mr. Smith many times... Thanks Dr. K.

RÉSUMÉ

La combustion et l'efficacité des piles à combustible sont les principaux problèmes auxquels plusieurs scientifiques se sont penchés. L'efficacité des piles peut en partie être améliorée en augmentant le transport de charges (électrons) du catalyseur à l'extrémité de l'anode.

Une première solution envisageable pour améliorer le transport des électrons du support poreux à l'extrémité de l'anode est de remplacer le noir de carbone par des nanotubes de carbone (CNTs). Étant donné que les CNTs ont une conduction électrique exceptionnelle, les électrons issue de la réaction pourront être transportés directement vers l'extrémité de l'anode en évitant plusieurs processus de marche aléatoire. Cet effet pourra d'autant plus être amplifié si les CNTs sont connectés directement à l'extrémité de l'anode par des liaisons chimiques.

À fin d'étudier la fonctionalisation des CNTs avec des outils numériques de chimie quantique, on doit faire un choix approprié des modèles à étudier. Étant donné que l'on s'intéresse essentiellement qu'aux propriétés des liaisons chimiques (longueur des liens et énergie de liaison) du groupe fonctionnel, on peut utiliser un plus petit modèle mais fiable pour représenter un CNT.

Le résultat le plus important de notre étude sur les groupes fonctionnels est que les accepteurs (CN, $Si(OH)_3$, COOH) ont un ordre et une énergie de liaison plus grandes que les donneurs (OH, NH_2, SiH_3). Nos résultats numériques montrent que les particules de platine sont fortement stabilisées par ces groupes fonctionnels aux énergies de liaison qui s'élèvent jusqu'à 3.14 eV et aux ordres de liaison allant jusqu'à 2. En comparant ces résultats avec le cas d'une particule de platine directement déposée au-dessus d'une molécule de pyrène, nos calculs montrent une

faible énergie de liaison de 1.28 eV et une faible ordre liaison de 0.22. Conséquemment, la coalescence des particules métalliques peut être significativement réduite à l'aide de groupes fonctionnels. Nous avons classé les groupes fonctionnels selon leur capacité à stabiliser une particule métallique.

- Accepteurs: $Si(OH)_3 > COOH > CN$
- Donneurs: $NH_2 > SiH_3 > OH$

Les résultats obtenus pour un petit modèle (pyrène) de nanotube de carbone mettent en évidence le bénéfice d'utiliser la fonctionalisation pour créer un site de germination pour les particules de platine.

ABSTRACT

The coalescence of the active phase of the catalyst used in fuel cells (Pt deposited over carbon black) represents a major drawback of this technology. Once the fuel cell starts working, the temperature raises, and the small platinum particles have enough energy to diffuse toward other particles in order to form larger particles, and consequently reduce both the active surface area and the reaction yield.

A plausible solution to this problem is to use functionalized carbon nanotubes as a support for the platinum particles. Instead of bonding platinum directly to the carbon support, the particles can be anchored to carbon nanotube through functional groups. The role of functional groups is to stabilize and fix platinum particles through the formation of stronger bonds between the Pt and the surface of the support. By changing from carbon black to carbon nanotubes, we also benefit from the high electrical conductivity of carbon nanotubes. They could facilitate the electron transport from the Pt particles to the back plane of the anode, creating an electron channel directly to the backplane. Therefore, limiting the random process of charge hopping in complex media.

Due to the large size of carbon nanotubes, computational chemistry calculations become impractical on representative models. Pyrene molecule represents a very good, but minimal model of a carbon nanotube, since it contains carbon atoms that resemble those present in carbon nanotubes. The central carbon atoms in pyrene have the same hybridization and the same chemical environment than in carbon nanotube, which makes pyrene the ideal candidate to investigate a large number of functional groups. We have chosen to simulate six different functional groups, they can be classified depending upon their electronic configurations in electron attractors and electron donors. We have selected commonly used with very well

known characteristics organometallic ligands. Among the selected there are three electron attractors (CN, $Si(OH)_3$, COOH) and three electron donors groups (NH_2, SiH_3, OH). We also explored the bonding of three different metal atoms (Platinum, Palladium and Nickel) to all functional groups, this allowed us to compare the stabilities of metals of the same group of the periodic table.

Our most important result for the investigated functional groups is that the attractors (CN, $Si(OH)_3$, COOH) have greater bonding energies and higher bond orders than the donors (OH, NH_2, SiH_3). Our computational results show that platinum particles are strongly stabilized by the functional group where bonding energy values up to 3.14 eV and bond orders up 2 were obtained. If we compare these results with platinum particles deposited directly over pyrene, our calculations showed energy of 1.28 eV and low bond order of 0.22. Therefore, the coalescence can be dramatically reduced when the metallic particles are bonded to functional groups. We have classified the functional groups accordingly to their ability to stabilize the metal particles:

- Attractors: $Si(OH)_3 > COOH > CN$
- Donors: $NH_2 > SiH_3 > OH$

The results obtained on a small model (pyrene) of a carbon nanotube give clear evidence of the benefit of using functionalization to create nucleation sites where Pt particles can be grown.

CONDENSÉ EN FRANÇAIS

C1 Pile à combustible

C1.1 Bref historique

En 1839, William Grove découvre comment générer de l'électricité à l'aide d'une réaction chimique impliquant uniquement de l'hydrogène et de l'oxygène dans un processus inverse de l'électrolyse de l'eau (Grove, 1839). Cette expérience disposait de deux tubes tests contenant chacune une électrode de platine à moitié plongées dans une solution aqueuse de H_2SO_4. Ensuite, on remplissait l'un des tube avec un gaz de H_2 et l'autre tube avec un gaz de O_2. Dès le commencement de la réaction, un galvanomètre détecta entre chaque électrode un courant électrique; c'est ainsi qu'est née la première pile à combustible.

C1.2 Problématique des piles à combustible actuelle

La combustion et l'efficacité des piles à combustible sont les principaux problèmes auxquels plusieurs scientifiques se sont penchés. L'efficacité des piles peut en partie être améliorée en augmentant le transport de charges (électrons) du catalyseur à l'extrémité de l'anode. Habituellement, le catalyseur est constitué de petites agrégats de platine déposés sur du noir de carbone (Peuckert et al., 1986; Uchida et al., 1996). Dès qu'une molécule de H_2 dissocie au contact du métal, les électrons produits suivent une trajectoire aléatoire au travers un support poreux de noir de carbone jusqu'à ce qu'ils atteignent l'extrémité de l'anode (Figure 1.4). À cause de ce processus de marche aléatoire des électrons, une grande partie de la charge disponible ne contribue pas à la production de l'électricité. De plus, lorsque la pile à combustible est mise en fonction, la température augmente ce qui affaiblie les liens entre le platine et le noir de carbone et favorise la coalescence des petites agrégats de platine. Les gros agrégats de platine ainsi formés diminuent la surface efficace

du platine nécessaire à la réaction et décroît l'efficacité de la pile à combustible (Figure 1.5).

C1.3 Solutions proposées et méthodologie

Une première solution envisageable pour améliorer le transport des électrons du support poreux à l'extrémité de l'anode est de remplacer le noir de carbone par des nanotubes de carbone (CNTs). Étant donné que les CNTs ont une conduction électrique exceptionnelle, les électrons issue de la réaction pourront être transportés directement vers l'extrémité de l'anode en évitant plusieurs processus de marche aléatoire. Cet effet pourra d'autant plus être amplifié si les CNTs sont connectés directement à l'extrémité de l'anode par des liaisons chimiques. Deuxièmement, la présence de groupes fonctionnels sur le support pourrait stabiliser les agrégats de platine et prévenir leur coalescence. Comme l'illustre la Figure 1.6, une solution optimale consisterait à combiner un support de CNTs avec des groupes fonctionnels stabilisateurs de platine.

À fin d'étudier la fonctionalisation des CNTs avec des outils numériques de chimie quantique, on doit faire un choix approprié des modèles à étudier. Étant donné que l'on s'intéresse essentiellement qu'aux propriétés des liaisons chimiques (longueur des liens et énergie de liaison) du groupe fonctionnel, on peut utiliser un plus petit modèle mais fiable pour représenter un CNT. Ceci permet d'étudier un plus grand nombre de cas de fonctionalisation en un temps de calcul plus court que si l'on utilisait un modèle plus complet de CNT. Pour ce faire, le choix du modèle s'est arrêté à la fonctionalisation d'une molécule de pyrène qui est une molécule plane fortement conjuguée dont les électrons π sont délocalisés de manière similaire que le graphène et le CNT. Afin de minimiser les effets aux frontières où les carbones de la périphérie n'ont normalement pas les trois carbones voisins sp^2, on se concentrera que sur les atomes de carbone du centre de la molécule. À l'aide de calculs $ab - initio$, plusieurs groupes fonctionnels seront étudiés pour ensuite explorer leurs

capacités à stabiliser des atomes et de petits agrégats métalliques.

C2 Revue de littérature

La recherche sur le développement d'une nouvelle génération de piles à combustible n'a pu ignorer les avantageuses contributions de la nanoscience telles que l'utilisation de nanostructures comme les nanotubes de carbones aux propriétés de conduction électrique exceptionnelle.

C2.1 Fonctionalisation des nanostructures de carbone

La fonctionalisation est une réaction chimique réalisée pour attaché un atome (ou un agrégat d'atomes) à une molécule ou à un système plus complexe. L'ajout de ce nouveau groupe permet de modifier quelques propriétés moléculaires bien précises, telles que la température de fusion, le moment dipolaire, et etc.

C2.2 Fonctionalisation des nanotubes de carbone monoparois (SWCNT)

La fonctionalisation des SWCNT est présentement classifié en cinq principaux groupes (Hirsch, 2002):

- Défauts structuraux (Defect-group)
- Parois covalente (Covalent sidewall)
- Exohèdral non-covalent avec tensioactifs (Non-covalent exohedral with surfactants)
- Exohèdral non-covalent avec polymères (Non-covalent exohedral with polymers)
- Endohèdral (Endohedral)

C2.2.1 Fonctionalisation d'une parois covalente

On s'attend à ce que les parois d'un SWCNT soit inerte. La principale raison pour ceci est due à la haute coordination des carbones sp^2 qui s'apparentent au graphène. Quand les nanotubes sont oxydés pour retirer les particules catalytiques, quelques défauts sont créés sur la parois saturée par des groupements acides (COOH). De tels fonctionalisations ouvre la route à d'autres types de réaction telle que l'halogénation (Mickelson et al., 1998) (voir la Figure 2.2-B pour une représentation). D'autres fonctionalisations de la parois peuvent être réalisées à l'aide de carbènes nucléophiles très réactifs (Holzinger et al., 2001). Dans une autre étude (Bahr et al., 2001), une électrode a été construite à l'aide d'un film de SWCNT. Suite à une réduction d'un sel d'aryle-diozonium sur le film de nanotubes, des groupes aryles restent attachés aux parois du SWCNT (voir la Figure 2.3).

C3 Méthodologie numérique

C3.1 Théorie de la fonctionnelle de la densité (DFT)

L'équation de Schrödinger (3.1) peut servir à décrire la densité électronique d'un atome, d'une molécule ou d'un solide. Si Ψ est la function d'onde qui décrit entièrement le système étudié, alors la valeur propre calculée de l'opérateur Hamiltonien $\hat{H}$ représente son énergie totale (E_{tot}) (Szabo and Ostlund, 1996a).

Parmi les nombreuses approches pour résoudre l'équation de Schrödinger, il y en a une largement utilisée qui utilise l'approximation Hartree-Fock (HF) (Szabo and Ostlund, 1996b) basée sur une méthode variationnelle. La méthodologie de HF est fondée sur la supposition qu'un seul déterminant de Slater peut décrire complètement la fonction d'onde à N-corps du système étudié. Ensuite, le calcul variationnel produira un ensemble de N équations différentielles à résoudre.

C3.2 Logiciel

Dans ce projet de recherche, on utilise le logiciel de chimie numérique Gaussian 03 (Frisch et al., 2004) qui est la plus récente version commerciale du code originalement développé par J. Pople. Les résultats produits par le logiciel Gaussian sont largement acceptés par la communauté scientifique étant donné ses multiples fonctions implémentées et sa grande utilisation parmi les scientifiques en chimie-physique numérique.

Lorsque la fonction d'onde est connue, plusieurs propriétés moléculaires peuvent être évaluées en performant diverses routines *ab-initio* (Foresman and Frisch, 1996a). Dans le cadre de cette maîtrise, des calculs d'optimisation de géométrie, de transfert de charge et d'ordre de liaison ont été réalisés.

C3.3 Du pyrène au nanotube de carbone multiparois (MWCNT)

Étant donné que les MWCNT sont des molécules pouvant facilement contenir plusieurs millions d'atomes (voir la Figure 3.2), réaliser des calculs DFT sur de tels systèmes est quasi impossible. Pour y remédier, on doit utiliser un plus petit modèle qui imite les propriétés du CNT et qui permettra d'explorer plusieurs groupes fonctionnels dans un temps raisonnable. Même un nanotube de carbone monoparois (SWCNT) est un système trop complexe pour être traité par calculs DFT en un temps raisonnable. Donc, une solution plus drastique mais réaliste est de considérer une molécule de pyrène comme une sous-unité d'un nanotube de carbone (voir la Figure 3.3). Par ce choix, on doit poser quelques importantes hypothèses. Premièrement, on considère que la parois intérieure du SWCNT ne procure pas de sites de réaction. Deuxièmement, on ne considère pas les interactions à longue portée dans la réaction et on se limite à une étude locale des propriétés chimiques. Toutefois, un modèle de la taille du pyrène permet l'étude de plusieurs groupes fonctionnels en un temps raisonnable. Étant donné que les

atomes de carbone au centre de la molécule de pyrène ont une coordination (3) similaire aux carbones d'un CNT, la réactivité de ces atomes de carbone devrait se rapprocher de ceux d'un CNT.

C4 Résultats sur la fonctionalisation du pyrène

Les groupes fonctionnels choisis pour cette recherche ainsi qu'un résumé des résultats sont présentés dans cette section.

C4.1 Groupes fonctionnels

C4.1.1 Accepteurs d'électron

Les accepteurs d'électron sont définit comme des systèmes moléculaires capables d'attirer une densité d'électron. Si un accepteur d'électron est utilisé pour fonctionaliser le pyrène, alors on peut s'attendre à un transfert de charge vers le groupe fonctionnel. Dans ce travail, ce sont les groupes suivant qui furent considérés: CN, $Si(OH)_3$ et COOH (voir la Figure 4.4).

C4.1.2 Donneurs d'électron

À l'inverse, les donneurs d'électron sont des systèmes moléculaires qui octroie une densité d'électron. Dans ce travail, ce sont les groupes suivant qui furent considérés: NH_2, SiH_3 et OH (voir la Figure 4.5).

C4.2 Fonctionalisation du pyrène

Deux types de cas de fonctionalisation du pyrène ont été considérés: le *cis* où les deux groupes fonctionnels se retrouvent du même côté du pyrène et le *trans* où chaque groupe fonctionel se retrouve de chaque côté du plan de la molécule. Après des calculs d'optimisation de géométrie, on évalue les énergies de liaison, les distributions de charges, les caractères liants et les paramètres structuraux. Chaque

cas d'isomère *cis* et *trans* a été étudié à l'aide de deux groupes fonctionnels identiques (homofonctionnel) ou d'un groupe fonctionnel avec un atome d'hydrogène (hétérofonctionnel). En guise d'illustration, la Figure 4.6 présente les cas d'isomères homofonctionnels *cis* et *trans* avec des groupes CN. Tandis que la Figure 4.7 illustre les cas des isomères hétérofonctionnels *cis* et *trans* avec un groupe fonctionnel NH_2. La Figure 4.8 montre les deux sites de fonctionalisation portant l'étiquette 4 et 8 caractérisés par des atomes de carbone formant des liaisons sp^2 avec ses voisins. Tout les angles diédraux présentés dans ce travail sont calculés à partir des 4 atomes de carbone étiquettés 4, 5, 8 et 9.

C4.3 Résultats pour le cas homofonctionnel

C4.3.1 Énergie de liaison

La Table 4.1 présente les énergies de liaison calculées pour les isomères *cis* et *trans*. On remarque que les complexes *trans* sont légèrement plus stable que ceux *cis*, avec comme seule exception le groupe $Si(OH)_3$. Le Tableau 4.2 montre les angles diédraux calculés, le pourcentage et l'énergie de déformation de la molécule de pyrène suite à sa fonctionalisation. Le pourcentage de déformation des complexes *trans* sont très faibles étant donné leur nature symétrique qui procure des angles diédrals avoisinant les 180°. Néanmoins, l'énergie de déformation pour les complexes *trans* sont du même ordre de grandeur que ceux des complexes *cis* qui ont pourtant de forts pourcentages de déformation.

C4.3.2 Transfert de charge

Le Tableau 4.3 présente le transfert de charge net calculé; en haut, le transfert de charge pour les groupes donneurs: et en bas, pour les groupes accepteurs. Le signe négatif implique un gain de charges négatives (électrons) et un signe positif indique la perte de charges négatives par la molécule de pyrène.

C4.3.3 Ordre de liaison et propriétés structurales

Une analyse de l'ordre de liaison du pyrène montre que chaque lien carbone-carbone a une valeur de 1.4, ce qui est consistant avec le nature aromatique de la molécule. Une fois le pyrène fonctionalisé, les ordres de liaison peuvent changer (voir la Figure 4.11). En effet, les ordres de liaisons calculées montre des valeurs proches de 1.4 pour les liens entre les carbones de périphérie et des valeurs qui chutent près de 1.0 pour les liens impliquant un carbone central. Cette tendance est observée à la fois pour les complexes *cis* et *trans* étudié, et tout les ordres de liaison calculés sont répertoriées dans le Tableau 4.4. À partir de la Figure 4.11, on note que l'aromaticité est brisée au centre du pyrène fonctionalisé et que les liens carbone-carbone en périphérie conservent leur nature aromatique selon la théorie de Wiberg. On note un autre tendance dans le Tableau 4.4, les groupes fonctionnels plus volumineux comme $Si(OH)_3$ montrent des ordres de liaison plus faibles que les plus petits groupes comme CN peu importe si on est dans un cas de donneur ou d'accepteur. Un dernière observation montre que plus le transfert de charge est important plus l'ordre de liaison est petite.

C4.4 Résultats pour le cas hétérofonctionnel

C4.4.1 Énergie de liaison

Le Tableau 4.5 résume les énergies de liaisons calculées pour le complexe pyrèneH-R pour les cas *cis* et *trans*. Une première observation montre que les énergies de liaison sont plus forte pour le cas hétérofonctionnel que pour le cas homofonctionnel. Le Tableau 4.6 montre les angles diédraux calculés, le pourcentage et l'énergie de déformation de la molécule de pyrène suite à sa fonctionalisation. On observe que les déformations des complexes *trans* sont plus élevées que les changements obtenues dans le cas homofonctionnel des complexes *trans*. Cette différence est simplement due au fait que la déformation exercée sur le pyrène soit non symétrique avec ses

groupes R + H, et donc, la perturbation n'est pas aussi également distribuée.

C4.4.2 Transfert de charge

Le Tableau 4.7 résume les transferts de charge calculés pour le complexe pyrèneH-R pour les cas *cis* et *trans*. Étant donné la différence d'électronégativité entre les atomes de carbone et d'hydrogène, on s'attendrait à observer un transfert de charge de l'hydrogène vers le carbone en position 8, mais cette tendance n'est observé que pour le cas impliquant des donneurs.

C4.4.3 Ordre de liaison et propriétés structurales

En comparant les ordres de liaisons du cas hétérofonctionnel (Tableau 4.8) avec ceux du cas homofonctionnel (Tableau 4.4), on obtient des résultats similaires à la fois pour les complexes *cis* et *trans*.

C5 Résultats sur la stabilisation des agrégats métalliques

Afin d'étudier la liaison entre des agrégats métalliques (Pt, Ni et Pd) avec le pyrène via un groupe fonctionnel, on a tout d'abord choisi comme point de départ la molécule de pyrène fonctionalisée. Dans cette série de calculs, on a permis aux agrégats métalliques, aux groupes fonctionnels et aux atomes centraux du pyrène à relaxer tout en fixant les autres atomes du système. Dans ce travail, on définie la stabilisation du métal comme étant l'énergie requise pour dissocier un seul atome (ou un agrégat) de métal au complexe. En guise d'énergie de référence, on compare la stabilisation avec l'énergie de liaison entre un agrégat métallique directement attaché aux atomes de carbone centraux du pyrène. Cette énergie de référence se rapproche de l'état actuel des piles à combustible où les agrégats de platine sont directement déposés sur le noir de carbone. Dans ce travail, la stabilisation a été évalué pour le cas homofonctionnel en considérant l'ajout soit d'un seul atome

métallique ou d'un seul dimère métallique.

C5.1 Systèmes à un atome métallique

C5.1.1 Énergie de référence

Comme mentionné plus haut, l'énergie de référence représente l'énergie du lien ponté entre un atome métallique avec les atomes de carbone au centre du pyrène tel que schématisé dans la Figure 5.1. À partir du Tableau 5.1, on remarque que les atomes métalliques sont faiblement liés au pyrène, ce qui suggère que les atomes métalliques peuvent se déplacer plus librement en surface de la molécule. L'évaluation de l'ordre de liaison entre l'atome métallique et les carbones en position 4 et 8 sont faibles, ce qui supposent aussi de faibles liaisons.

C5.1.2 Groupes fonctionnels

Les ordres de liaison pour le métal-carbone (liens en position 4 et 8) sont petites ce qui implique que les liaisons formées soient faibles. De façon générale, les énergies de liaison calculées pour les groupes donneurs sont faibles et suggèrent la formation de liens faibles. Par contre, les groupes accepteurs montre de fortes énergies de liaison synonyme de liaisons fortes. Les principales variations de charge se limitent au niveau des groupes fonctionnels et de l'atome métallique, et non au reste de la molécule.

C5.2 Systèmes à un dimère métallique

Un exemple de stabilisation d'un dimère métallique via un groupe fonctionnel est présenté dans la Figure 5.3. Dans cette configuration, seulement un atome du dimère est lié aux groupes fonctionnels. Ce modèle ressemble à celui d'un atome métallique mais avec l'ajout d'une liaison métal-métal. Le Tableau 5.4 résume les énergies de liaison calculées pour les systèmes impliquant le dimère métallique.

Comme précédemment, les groupes fonctionnels, les atomes de carbone en position 4 et 8 et le dimère métallique ont été relaxés dans un calcul d'optimisation de géométrie. La distance entre les deux atomes métalliques a été fixée à la valeur obtenue pour le cas d'un dimère isolé.

C6 Conclusions

D'après le travail réalisé durant ce mémoire, on arrive aux conclusions suivantes:

- La molécule de pyrène est le plus petit modèle possible pour représenter un nanotube de carbone; les atomes de carbone en position 4 et 8 ont un environnement chimique similaire à ceux retrouvés dans un nanotube de carbone.
- Les groupes accepteurs étudiés (CN, $Si(OH)_3$, COOH) ont de plus grandes valeurs d'énergie et d'ordre de liaison que ceux des groupes donneurs (OH, NH_2, SiH_3).
- À la fois l'homofonctionalisation et l'hétérofonctionalistion ont montré la même tendance en terme de "force" de liaison avec le pyrène.
- Si un agrégat métallique est adsorbé sur le pyrène via un groupe fonctionnel, les valeurs d'énergie et d'ordre de liaison seront plus grandes que lorsqu'aucun groupe fonctionnel n'est en jeu. Donc, les agrégats métalliques sont mieux stabilisés à l'aide d'un pyrène fonctionalisé.
- Lorsque les agrégats métalliques sont stabilisés sur le pyrène, la densité électronique tend à s'accumuler sur le pyrène. Ceci suggère que durant la réaction anodique d'une pile à combustible, les électrons issus de la dissociation de la molécule d'hydrogène pourront être plus facilement conduits vers le support.
- Parmi les métaux et groupes fonctionnels étudiés, on obtient que le nickel possède les plus faibles valeurs d'énergie et d'ordre de liaison, tandis que le

platine obtient les plus fortes valeurs.

- Malgré une brisure d'aromaticité au centre du pyrène produite à la suite de la fonctionalisation, les liens conjugés $\pi - \pi$ sont essentiellement conservés en périphérie de la molécule.

Afin de poursuivre ce projet de recherche, plusieurs points pourront être considérés. Entre autre, on pourrait modéliser la dissociation de la molécule d'hydrogène en contact avec l'agrégat métallique. Ensuite, il faudrait étudier le transfert de charge dû à la dissociation de l'hydrogène vers les anneaux du pyrène via les groupes fonctionnels. D'autre part, on pourrait considérer un modèle plus gros que le pyrène tel que le coronène afin de confirmer les tendances observées dans cette recherche. Finalement, lorsqu'un modèle complet de SWCNT sera utilisé, il faudra évaluer l'influence de la fonctionalisation sur le caractère métallique et semi-conducteur du nanotube.

TABLE OF CONTENT

LIST OF FIGURES

LIST OF SYMBOLS AND ABREVIATIONS

$\psi(t)$: Time dependant wavefunction

Abreviations

DFT: Density Functional Theory

HF: Hartree-Fock

SCF: Self-Consistent-Field

CNT: Carbon Nanotubes

$SWCNT$: Single-Wall Carbon Nanotube

$MWCNT$: Multi-Wall Carbon Nanotube

FC: Fuel Cell

$PEMFC$: Proton Exchange Membrane Fuel Cell

$CHPG$: Combined Heat and Power Generation

BE: Bonding Energy

LDA: Local Density Aproximation

GGA: Generalized Gradient Approximation

$a.u$: Atomic Units definitions:

Quantity	Name	Symbol	Value in SI
Length	Bohr radius	a_0	5.292 x10^{-11} m
Mass	Electron rest mass	m_e	9.109 x10^{-31} kg
Charge	Elementary charge	e	1.602 x10^{-19} C
Angular momentum	Planck's constant	$\hbar = h/2\pi$	1.054 x10^{-34} Js^{-1}
Energy	Hartree energy	E_h	4.360 x10^{-18} J
Electrostatic const.	Coulomb's constant	$1/(4\pi\epsilon\theta)$	8.988 x10^{9} $C^{-2}Nm^2$

LIST OF TABLES

CHAPTER 1

INTRODUCTION

1.1 Fuel cells

1.1.1 Short history

In 1839, William Grove realized how to generate electricity from a chemical reaction involving only hydrogen and oxygen by reversing water electrolysis (Grove, 1839). Two test tubes containing Platinum electrodes were half immersed in an aqueous solution of H_2SO_4. The first tube was then filled with gaseous H_2, and the second one with O_2. As the reaction began, a connected galvanometer was able to detect the electron flow; the first fuel cell was born. This first experimental setup received the name "Gaseous Voltaic Battery" and was not, until 1922, called a fuel cell. (Rideal and Evans, 1922)

In 1962, fuel cells (FC) provided power and drinkable water to the Apollo space mission service module. Then in 1965, they were used as the main source of power for a two persons electric car used during Gemini space mission to explore the surface of the moon.

In 1966, General Motors (GM) was presenting the first electrical vehicle ever built (GeneralMotors, 2006), it was known as "The Electrovan". Although they never made the line of production, this has demonstrated the feasibility of building a propulsion system using only electrical power that is provided by an alkaline fuel cell.

Modern fuel cells such as those industrially developed by *Ballard Power Systems*, are now used in buses (Chen, 2003) in Berlin (Germany), as well as in some "exhibition" cars. This can be considered as a step towards alternative propulsion energy sources.

1.1.2 Classification of fuel cells

Fuel cells are electrochemical reactors that are able to convert chemical energy into electrical energy. They behave as batteries able to generate power from a chemical reaction, or as engines as long as the fuel is available.

Certain kinds of fuel cells, such of those using H_2 as fuel, will only produce water and energy. This may represent a suitable answer for "green" energy generation for the years to come. They could also be used to produce drinkable water in remote areas, where water pipelines would be very expensive to build and maintain, due to geographic difficulties. Fuel cells are convenient solutions for heat and power generation in regions where standard power grids are not easily available *i.e.* for boats, motor homes, remote scientific stations, etc.

Among all kinds of fuel cells, there are five major groups (Hoogers, 2003a) which are based on the different type of electrolyte used. Some of their properties are summarized in Table 1.1. By inspecting Table 1.1, we notice that in combination with their generated power, a further classification can be done; low (<150 °C), medium (150 - 500 °C) and high (>500 °C) operation temperature. Among low and medium temperature groups, only H_2 is used as fuel, while in the high temperature group H_2, CH_3OH, and CH_4 can be used as fuels. The operation temperature plays an important role since it will determine the applications of the FC.

Table 1.1 Properties of the different kinds of fuel cells.

Type	Electrolyte	Charge Carrier	Operation Temperature	Fuel
Alkaline	KOH	OH^-	(60-120) °C	H_2
PEMFC	Solid Polymer	H^+	(50-100) °C	H_2
H_3PO_4 FC	H_3PO_4	H^+	~220 °C	H_2
Carbonate FC	$K_2/Li_2(CO)_3$	$(CO)_3^{2-}$	~650 °C	H_2, CH_3OH, CH_4
Solid Oxide FC	ZrO_2, Y_2O_3	O^{2-}	~1000 °C	H_2, CH_3OH, CH_4

1.1.3 Applications of fuel cells

Different areas of technology may profit from the use of FC, that differ from the amount of energy needed and produced. Table 1.2 shows some general applications[1] of fuel cells.

Table 1.2 FC generated power and application range.

Type	Efficiency	Power	Application
Alkaline	(35-55)%	< 5 kW	Military, Space
PEMFC	(35-45)%	(5-250) kW	Automotive, CHPG
H_3PO_4 FC	40%	200 kW	CHPG
Carbonate FC	>50%	200 kW - 200 MW	CHPG, Stand Alone
Solid Oxide FC	>50%	2 kW - 2 MW	CHPG, Stand Alone

We can notice that higher operation temperatures, imply higher amounts of generated power. We can also see that due to engineering issues in FC, an average of 50% of the chemical energy is successfully transformed into electricity. This is specially true for the H_2 fueled ones. The main problem of H_2 FC lays on the fact that H_2 generally needs to be generated in a separate process. Moreover, a constant source of hydrogen needs to be attached nearby the FC. Hence, fueling becomes an impor-

[1] Where CHPG stands for Combined Heat and Power Generation

tant drawback. In vehicles, hydrogen is stored in tanks in a gaseous state. The H_2 liquefaction requires cryogenic tanks (Hoogers, 2003b), and there is an extra energy consumption to perform the liquefaction. Despite the fueling problem, the main advantage is that low temperature FC are able to produce electricity immediately after its starts. They appear quite suitable for transportation applications where multiple "starts" and "stops" may occur.

On the other hand, the main problem of the high temperature FC group is not related to the fuel, but rather to the operation mode since they can not be turned off easily. Therefore, they appear more suitable for generation of amounts of electricity large enough to provide small facilities or populations located in remote areas. Their high working temperature will necessitate a certain amount of time before being reached.

1.1.4 Fuel cell components and chemical reactions

Fuel cells are made of four main parts: the anode, the cathode, the catalyst and the exchange proton membrane. See figure 1.1[2]

The anode It is the material on which the fuel (H_2) gets oxidized into an electron (e^-) and a proton (H^+). An example of anodic reaction (if H_2 is used as fuel) is shown below:

$$H_2 \overset{catalyst}{\longrightarrow} 2H^+ + 2e^- \tag{1.1}$$

The H_2 molecule is oxidized into protons (H^+) and generates electrons. For this reaction to take place, a catalyst is usually used.

[2]taken from: http://www.cramscience.ca/es.php?a=52

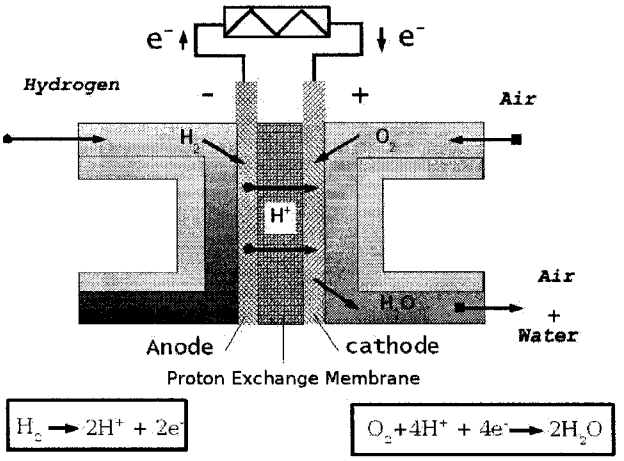

Figure 1.1 Schematic representation of a fuel cell.

The cathode It is the material where the oxygen is reduced. After protons arrive at the cathode, a chemical reaction known as the cathodic reaction occurs. A typical cathodic reaction is:

$$O_2 + 4H^+ + 4e^- \overset{catalyst}{\longrightarrow} 2H_2O \tag{1.2}$$

In general, oxygen in this reaction comes from air. A catalyst is also used to facilitate this reaction.

Among the materials available for both anode and cathode (electrodes) we have:

- Raney nickel. (mixtures of fine grains of nickel or silver and aluminum)
- Palladium.
- Carbon.

The Catalyst It is located in both anode and cathode. The catalyst role is to provide an alternative path for the chemical reaction. In general, they decrease the reaction activation energy, therefore the chemical reactions can occur faster and more efficiently.

The Proton Exchange Membrane (PEM) It blocks the electron (e^-) coming from the anode, and allows the proton (H^+) to flow in the direction of the cathode. PEM are made from perfluorinated polymers trademarks of Dupont and Dow Chemical. In Figure 1.2 both structures are shown.

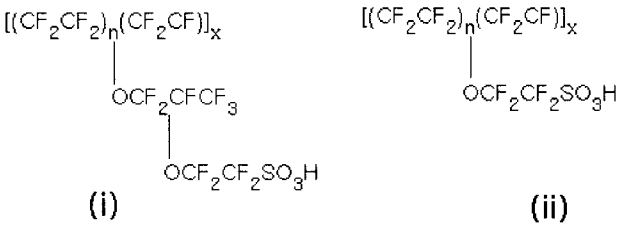

Figure 1.2 Structure of perfluorinated polymers (i) Nafion^{TM} (ii) Dow Chemical.

Modern polymers like BAM3G (a trademark of Ballard System) are new materials that constitute alternative types of membrane. They cost less and have greater performance. The structure of this polymer is shown in Figure 1.3.

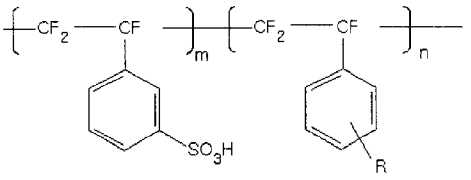

Figure 1.3 Structure of the BAM3G polymer.

We may resume the FC device as follows. The flow of H_2 gas is directed to the anode, once it is in contact with the catalyst, the H_2 molecule splits, electrons are driven out of the reactor and are used to perform an electrical work. Meanwhile, the H^+ flows through the proton exchange membrane until it reaches the cathode. Returning electrons flow into the cathode to meet with the flow of oxygen coming into it. At the cathode, the final chemical reaction takes place to produce H_2O, which is taken out from the reactor.

The overall chemical reaction that occurs in a fuel cell:

$$2H_2(g) + O_2(g) \overset{catalyst}{\longrightarrow} 2H_2O(l) + \text{Energy} \tag{1.3}$$

1.2 Problems with actual fuel cells

As mentioned above, the fueling and the overall efficiency of fuel cells are among the more serious problems that need to be addressed. The efficiency could be improved by increasing charge (electron) transport from the catalyst to the anode backplane. The catalyst is built of small Pt particles deposited over carbon black (Peuckert et al., 1986; Uchida et al., 1996) Once the H_2 molecule is dissociated into atomic species, electrons produced follow a random trajectory through the porous carbon black support to reach the anode back plane (Figure 1.4). Because of this "random walk" charges need a certain amount of time to reach the cathode, due to multiple scattering events, trapped charges, etc. Therefore, overall process becomes very inefficient. In addition, once the FC starts working and the temperature raises, the platinum particles begin to coalesce due to the weak bonding between Pt and the carbon black support. The formation of larger Pt particles decreases the amount of surface Pt atoms available to catalyze the reaction, and decreases the efficiency of the fuel cell. (Figure 1.5)

1.3 Proposed solution and methodology

A plausible solution to improve the efficiency in electron transport into the porous materials through the anode is to use carbon nanotubes (CNTs) instead of carbon black. Since CNTs have exceptionally high electrical conductivity, the collected electrons may be transported more directly to the anode without going through

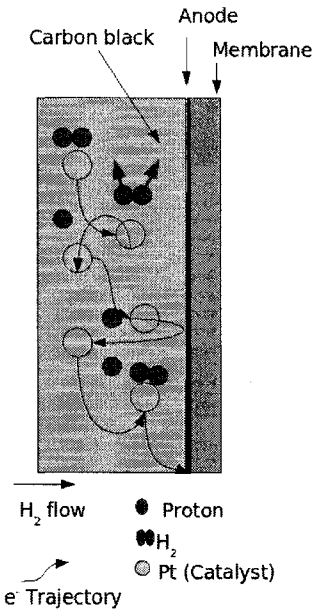

Figure 1.4 Charge random walk in the porous media.

these random processes. This could be even amplified if the carbon nanotubes are directly connected to the anode backplane by chemical bonds. Secondly, the presence of functional group on the support may stabilize the Pt particles and prevent their coalescence. On Figure 1.6, we show a schematic representation of the proposed solution.

This potential solution has been already investigated with Multi-wall carbon nanotubes (MWCNTs) by an experimental group at INRS. The first work shows that MWCNTs can be used as an electrode backplane, by growing MWCNTs on fibers from carbon black as support (Sun et al., 2004). A second publication (also from this group) gives an experimental procedure to deposit Pt nanoparticles over these grown MWCNT (Villers et al., 2006). Their electrodes are already more efficient for the oxidation reaction than the available commercial ones. We believe that FC overall efficiency can be further inverted, if the Pt nanoparticles are deposited on CNT via a functionalization group which could reduce the coalescence of Pt. In addition we could profit from the higher electrical conductivity of carbon nanotubes,

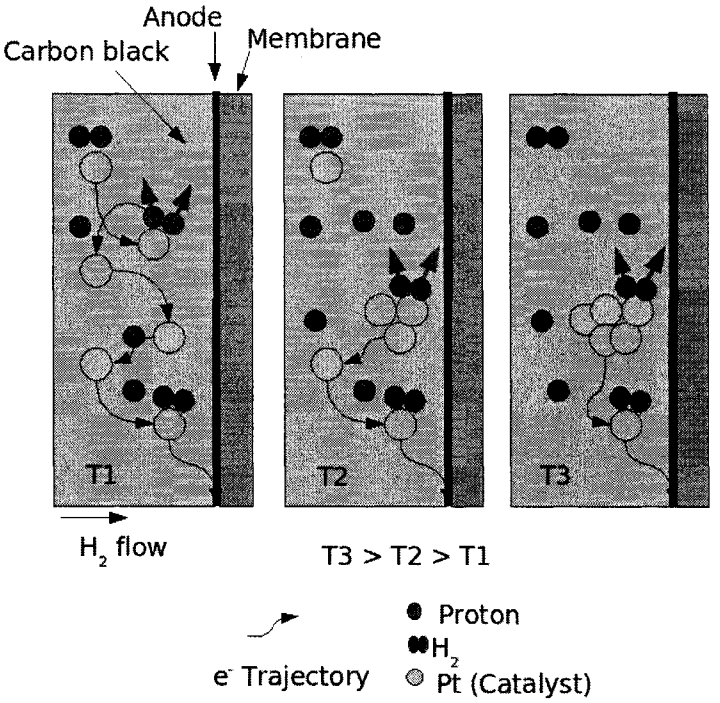

Figure 1.5 Representation of Pt coalescence.

therefore reducing the multiple scattering of the carrier along the diffusion path to the electrode.

In order to numerically study the functionalization of CNTs with quantum chemical tools, we have to make an appropriate choice for the models. In fact, since we are mostly interested by the bonding properties (bond length, bonding energy), we can use a small molecule that constitutes a fragment of a CNT model. This would allow us to investigate, several different functionalization scheme within a shorter computational time than if larger model was used.

We have then chosen to study the functionalization of the pyrene molecule, which is a highly conjugated and flat molecule where π electrons are delocalized in a similar manner that in graphene and carbon nanotubes. In order to minimize side effects where carbon atoms do not have the standard three sp^2 carbon neighbors, we will

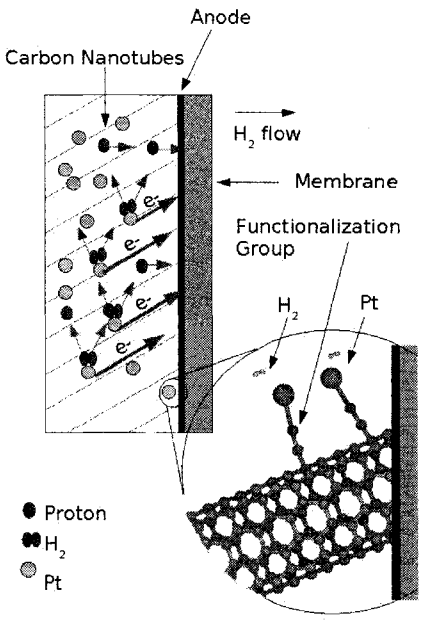

Figure 1.6 Pt functionalized CNT as catalyst support.

concentrate our study on the central carbon atoms.

Using first principles calculations, different functionalization groups on pyrene will be investigated. Then, the stability of metal atoms and clusters on this functionalized model will be explored. By comparing the different bonding energy and bond orders obtained from the calculations, we will be able to establish a tendency among the selected groups and metallic atoms.

1.4 Thesis structure

The thesis is built in the following manner. In Chapter II, we describe the more recent theoretical and experimental works in the field of carbon nanotubes functionalization. Also, we extend the discussion to the functionalization of carbon nanocomposites.

In Chapter III, the reader will find the computational description of the models. Density Functional Theory (DFT) will be briefly presented. A graphical representations of the models used will be presented and discussed in detail. Descriptions and justifications about the basis sets and the pseudopotentials used will be also given.

Chapters IV and V are devoted to the theoretical results obtained on pyrene functionalization and on the stabilization of different metal (Pt, Ni and Pd) particles.

A discussion of the results is carried out in Chapter VI, and is followed by some conclusions.

CHAPTER 2

LITERATURE SURVEY

Nanostructures are the target of intensive scientific research. They are present in many fields of research, we hear terms like "Nanoengineering", and it seems to be the engineering last frontier: *The ability to build something by using one atom at a time.* Fuel cells research, could not escape from this scientific revolution, and because of their excellent electronic conductivity, carbon nanotubes can now be explored as one of the answers in the quest of building better catalysts in future fuel cells. We must remember that the active area in a Proton Exchange Membrane Fuel Cell (PEMFC) is where Platinum particles are located, and where the H_2 gets splitted to release electrons.

2.1 Single wall carbon nanotube

A Single-Wall Carbon Nanotube (SWCNT) is often pictured as a graphene sheet rolled on itself to form a cylinder, with a diameter around $\sim$ 1-2 nm, and an aspect ratio (length/diameter) larger than 10^6. Because of this, carbon nanotubes (CNT) are considered as a perfect one dimensional system (Saito, 1998). By defining a chiral angle θ_0 over the plane of an unrolled CNT (see Figure 2.1)[1] a further classification of them can be given as:

- Achiral: the specular image and the CNT itself are structurally identical. Among them, two possible types:

[1]Image taken from: http://spie.org/Images/Graphics/Newsroom/Imported/0806

1. Armchair ($\theta_0 = 30°$)
2. Zigzag ($\theta_0 = 0°$)

- Chiral: its mirror image cannot be superposed ($0° \leq \mid \theta_0 \mid \leq 30°$).

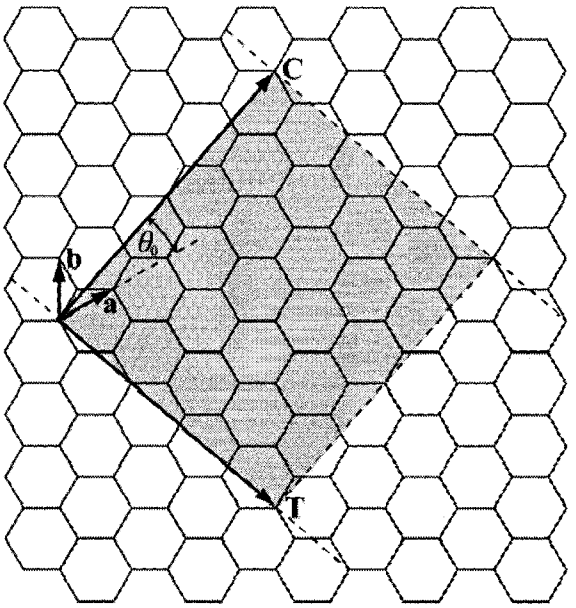

Figure 2.1 Classification of carbon nanotubes

The chiral vector (R) is defined as:

$$R = aT + bC \equiv (a, b), \tag{2.1}$$

where a and b are integers ($0 \leq \mid a \mid \leq b$), and satisfy

$$2a + b = 3n \tag{2.2}$$

If n is an integer, the CNT is metallic, otherwise it is semiconductor. Armchair (a=b) nanotubes are always metallic since π^* conduction and π valence bands overlap at the Fermi level (White et al., 1993). Zigzag tubes (a, 0) are semiconductors, but if n is a multiple of 3 then the zigzag will have a semi-metallic character.

Carbon nanotubes have exceptional electronic transport properties (Dresselhaus et al., 1992; Hamada et al., 1992; Mintmire et al., 1992) as well as outstanding mechanical properties (Salvetat et al., 1999). It has been proposed that CNT could also be implemented as an element in Proton Exchange Membranes (Wang et al., 2004) within fuel cells, due to their excellent electron transport capabilities.

One of the most interesting properties of carbon nanotubes is the high conductivity of metallic tubes. Ballistic transport can occur in carbon nanotubes (Li et al., 2005) if its length is comparable to the electronic mean free path. The conductance (G) is quantified by integer values of G_0.

$$G_0 = \frac{2e^2}{h} \tag{2.3}$$

where e is the electron charge and h is the Planck constant.

Metallic carbon nanotubes have a conductance of $2G_0$ at Fermi energy (E_f) where two conduction bands overlap (McEuen et al., 1999).

2.2 Functionalization of carbon nanostructures

A functionalization is a chemical reaction performed to attach or to anchor an atom (or group of atoms) to a molecule or a more complex system. This newly bonded group is responsible for changes in some specific molecular properties, such as the melting point, the dipole moment, etc. A simple example is the replacement of an hydrogen atom by a hydroxyl group in methane to form methanol. The melting point goes from -182.5 °C for methane to -97 °C for methanol, while the dipole moment goes respectively from 0 to 1.69 D.

2.2.1 Functionalization of SWCNT

Functionalization of SWCNT is presently classified into five main groups (Hirsch, 2002)

- Defect-group
- Covalent sidewall
- Non-covalent exohedral with surfactants
- Non-covalent exohedral with polymers
- Endohedral

2.2.1.1 Defect group functionalization

This kind of functionalization can occur during chemical purification of nanotubes. Carbon nanotubes can be grown using metallic particles as catalyst like Fe, Ni or Co. (Rao et al., 2001) When the metallic particles are removed using oxydative methods, CNTs are attacked by acids, creating a series of small and very reactive tubes (Hamon et al., 2001). These small tubes have defects on their sidewalls where reactions will easily happened. In figure 2.2-A we see a representation of this kind of functionalization[2].

2.2.1.2 Covalent sidewall functionalization

SWCNT sidewalls are expected to be inert. The main reason for this is due to the high coordination of sp^2 carbon that is very similar to graphene sheet. When

[2]Image 2.2 was taken from (Hirsch, 2002).

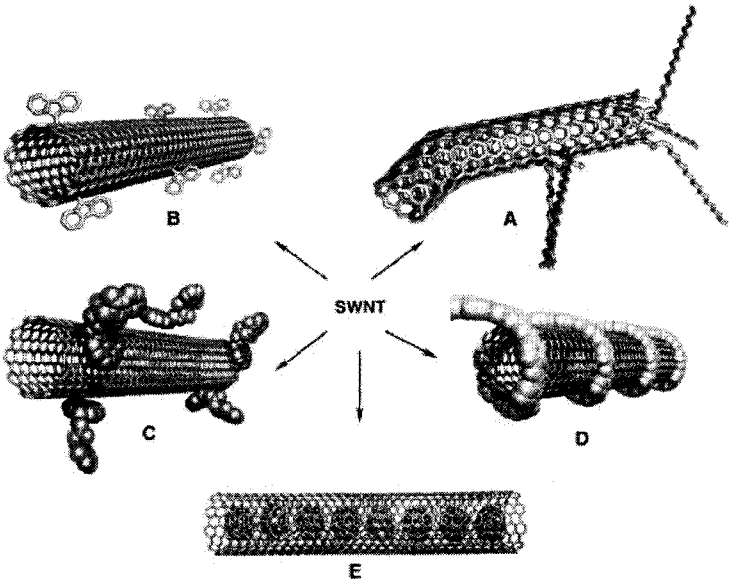

Figure 2.2 Schematic representation of carbon nanotubes functionalization. A) defect-group functionalization B) covalent sidewall functionalization, C) noncovalent exohedral functionalization with surfactants, D) noncovalent exohedral functionalization with polymers, and E) endohedral or "storage" functionalization.

the nanotubes are oxidized to remove the catalyst particles, some defects that are created on the walls can be saturated with acidic groups (COOH). Such functionalization opens the route to some other reactions like fluorination (Mickelson et al., 1998) (see the figure 2.2-B for a representation) to be performed. Other sidewall functionalization can be achieved using highly reactive nucleophilic carbenes (Holzinger et al., 2001). In a different study (Bahr et al., 2001), an electrode was built with SWCNT as a solid film called bucky paper. A reduction of aryldiazonium salt (see Figure 2.3) on this film was carried out, where the removal of the N_2 leaves the aryl groups attached to the SWCNT sidewall.

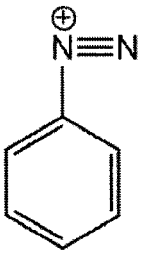

Figure 2.3 Schematic representation of aryl-diazonium cation.

2.2.1.3 Non-covalent exohedral functionalization

A non-covalent functionalization occurs when molecules form bonds without sharing a pair of electrons. The bond is formed trough other variety of interactions between them like π-π interactions. Experiments (Chen et al., 2001) have confirmed this kind of interaction between carbon nanotubes and the compound N-succinimidyl-1-pyrenebutanoate represented in figure 2.4, during a non destructive purification of the carbon nanotubes. In a different work (Krstic et al., 1998), SWCNT were found in the aqueous phase of sodium dodecylsulfate (SDS), a surface-active molecule (a substance capable of reducing the surface tension of a liquid in which it is dissolved) that can established strong π-π interactions. Figure 2.2-C shows a schematic representation of this kind of functionalization.

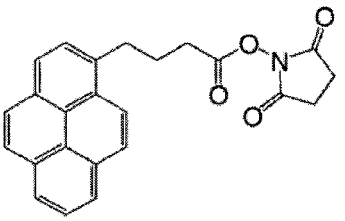

Figure 2.4 Schematic representation of N-succinimidyl-1-pyrenebutanoate

Polymers like poly m-phenylene-co-2,5-dioctoxy-p-phenylenevinylene (PmPV), (see figure 2.5) have also been used to functionalize SWCNT (Star et al., 2001). Atomic-

force Microscopy (AFM) experiments have shown that such polymer wraps the nanotube uniformly (see figure 2.2-D for a representation), forming supramolecular complexes. It was concluded from this work that the wrapping by the polymer changes dramatically the conductivity of the formed supramolecular complex, which becomes eight times higher after functionalization.

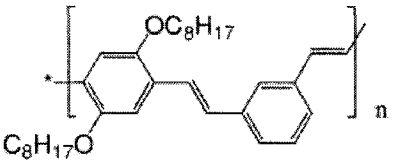

Figure 2.5 Schematic representation of PmPV polymer.

2.2.1.4 Endohedral functionalization

Endohedral functionalization is also known as "storage" functionalization. It is the functionalization of the interior of a carbon nanotube. Taken the CNT as a long cylinder, its inner cavity offers an interesting storage media for chemical species such as ionic crystals (Wilson and Madden, 2001), C_{60} (Smith et al., 1999) also called "bucky peapods" and metallofullerenes $Sm@C_{82}$ (Okazaki et al., 2001).

2.3 Pyrene

Pyrene is a polycyclic aromatic hydrocarbon (see Figure 2.6). It has four fused benzene rings that forms a planar aromatic system. Carbon atoms in pyrene are hybridized sp^2, thus showing an electronic delocalization on the p orbitals. It has a chemical formula of $C_{16}H_{10}$ and a molecular weight of 202.26 g/mol. Pure pyrene is a colorless crystalline solid at ambient temperature, and it is often commercially used to produce dyes, pesticides, and some plastics. Like most of polyaromatic

compounds, pyrene can be derived from coal tar. The structure of pyrene was first confirmed in 1945 (Robertson and White, 1945) using X-ray diffraction. By 1948, its electronic structure was studied theoretically (Moffitt and Coulson, 1948) in detail, using both molecular orbital as well as valence theory.

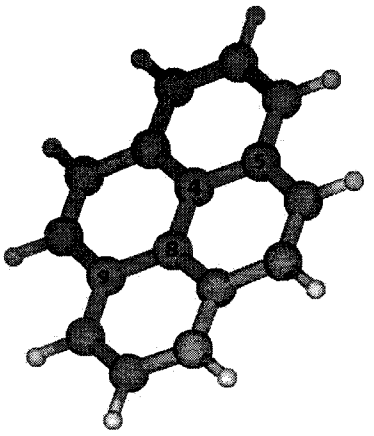

Figure 2.6 Schematic representation of a pyrene molecule.

2.3.1 Pyrene functionalization

The pyrene molecule appears more often as a functionalization group due to its propensity for $\pi - \pi$ stacking with carbon nanotubes (Chen et al., 2001). To our knowledge, there is no study that investigates both energetic and structural properties on the functionalization of pyrene. Some recent studies reveals specific features related to its electronic density (Hernandéz et al., 2004), also its structural properties using DFT (Park and Cheong, 2006). In another study that combines both theoretical and experimental approaches using configuration interaction (CI) and Raman spectroscopy respectively, authors have found an agreement, between theoretical and experimental frequencies and intensities of Raman measurements (Neugebauer et al., 2005).

2.3.2 Summary

We have seen that carbon nanotubes are systems under a heavy scientific investigation. Their functionalization have different trends, depending upon the answer they may offer; like endohedral functionalization used for "nanostorage" or sidewall functionalization to anchor chemical groups that change their properties. Since production of carbon nanotubes it is in its early stage of development, theoretical studies represents a feasible answer to study their properties in a less expensive way and much faster that rather conduct experiments directly on them.

To functionalize carbon nanotubes using the current computational methods, also represents a huge challenge. Direct calculations on them becomes impractical due to their size. That is why, we have chosen a small molecule to represent them: pyrene, which is a molecule that resembles carbon nanotubes. All of its carbon atoms have sp^2 hybridization, and two of them (central carbons) are chemically equivalent to those found in carbon nanotubes. Using pyrene as a model allow us to explore more chemical functionalizations in a reasonable time frame.

Our literature review shows that theoretical pyrene functionalization represents an innovative approach, since the subject has not been reported so far. This novel idea could offer fast and reliable answers about structural configurations, binding energies, bond orders among other molecular properties of functionalized carbon nanocomposites, since emerging trends could be probably extrapolated to the mentioned carbon nanocomposites of any size, including multiwalled carbon nanotubes.

CHAPTER 3

COMPUTATIONAL METHODOLOGY

In this chapter, we briefly introduce the Density Functional Theory (DFT). Then we describe the calculations that were performed during this research project. Finally, we give a short description of some capabilities of the computational chemistry software used.

3.1 Density Functional Theory (DFT)

The Schrödinger equation (3.1) can be used to describe the electronic density of an atom, a molecule or a solid. If Ψ is a wavefunction describing completely the system under study, then the computed *eigenvalues* of the Hamiltonian operator $\hat{H}$ represent all possible values of its total energy (E_{tot}) (Szabo and Ostlund, 1996a).

$$\hat{H}\Psi = E_{tot}\Psi \tag{3.1}$$

For a molecule having "N" electrons and "M" nuclei, the Hamiltonian operator is written (in atomic units):

$$\hat{H} = -\sum_{i=1}^{N}\frac{1}{2}\nabla_i^2 - \sum_{A=1}^{M}\frac{1}{2M_A}\nabla_A^2 - \sum_{i=1}^{N}\sum_{A=1}^{M}\frac{Z_A}{r_{iA}} + \sum_{i=1}^{N}\sum_{j>1}^{N}\frac{1}{r_{ij}} + \sum_{A=1}^{M}\sum_{B>A}^{M}\frac{Z_A Z_B}{R_{AB}} \tag{3.2}$$

where M_A is ratio of the mass of nucleus A to the mass of an electron, and Z_A is the atomic number of atom A, r_{ij} is the distance between the electrons i and j, and R_{AB} is the distance between nucleus A and B. In equation (3.2) the first two terms

are the kinetic energy of electrons and nuclei respectively, the third term accounts for the coulombic attraction between electrons and nuclei, the repulsion between electrons and nuclei are the fourth and fifth terms in the equation.

For a system that is composed of two particles, equation 3.1, in conjunction with equation 3.2 can be solved exactly using a central force approach. For systems involving more than two particles the equation becomes analytically unsolvable due to mathematical complexity. We then need to use approximations that help to overcome this mathematical "barrier". In that sense, the cornerstone of quantum chemistry and solid state physics is perhaps the Born-Oppenheimer approximation. It states that, since nuclei are much more heavier than electrons, they can be considered to be fixed as compared to electrons (Born and Oppenheimer, 1927). If we use this approximation, the complexity of the Hamiltonian operator ($\hat{H}$) is reduced dramatically since now it can be split into two different and independent Hamiltonians; the electronic Hamiltonian:

$$\hat{H}_{elec} = -\sum_{i=1}^{N} \frac{1}{2}\nabla_i^2 - \sum_{i=1}^{N}\sum_{A=1}^{M} \frac{Z_A}{r_{iA}} + \sum_{i=1}^{N}\sum_{j>1}^{N} \frac{1}{r_{ij}} \tag{3.3}$$

and the nuclear Hamiltonian:

$$\hat{H}_{nuc} = -\sum_{A=1}^{M} \frac{1}{2M_A}\nabla_A^2 + \sum_{A=1}^{M}\sum_{B>A}^{M} \frac{Z_A Z_B}{R_{AB}} \tag{3.4}$$

where the index "i" and "j" are related to electrons, index "A" is used for the nuclei. The total energy E_{tot} for fixed nucleus is defined by:

$$E_{tot} = E_{elec} + \sum_{A=1}^{M}\sum_{B>A}^{M} \frac{Z_A Z_B}{R_{AB}} \tag{3.5}$$

When these mentioned Hamiltonian operators (equations (3.3) and (3.4)), are applied to the correspondent "electronic" or "nuclei" wavefunctions, they will give *eigenvalues* as results. These are the electronic energy (E_{elect}) and the nuclei energy (E_{nuc}), respectively. See equations (3.6) and (3.7).

$$\hat{H}\Phi_{elec} = E_{elec}\Phi_{elec} \tag{3.6}$$

$$\hat{H}\Phi_{nuc} = E_{nuc}\Phi_{nuc} \tag{3.7}$$

There are different approaches to solve equations (3.6) and (3.7). A common approach is to use the Hartree-Fock (HF) approximation (Szabo and Ostlund, 1996b) that is based on the variational method. Starting with a trial wavefunction (χ), let us write the energy functional ($E[\chi]$) as,

$$E[\chi] = \langle\chi|H|\chi\rangle \tag{3.8}$$

Since $E[\chi]$ is a functional of χ, introducing the following variation of χ,

$$\chi \longrightarrow \chi + \delta\chi \tag{3.9}$$

will impact over the energy in such a way that it will become,

$$E[\chi + \delta\chi] = E[\chi] + \delta E + \ldots \tag{3.10}$$

where δE is the first variation in E. The goal of this variational procedure is to

find $\delta\chi$ that gives $\delta E = 0$. This variation is carried out in a procedure called Self-Consistent-Field (SCF) calculation. Figure 3.1 shows an schematic flow chart of the procedure.

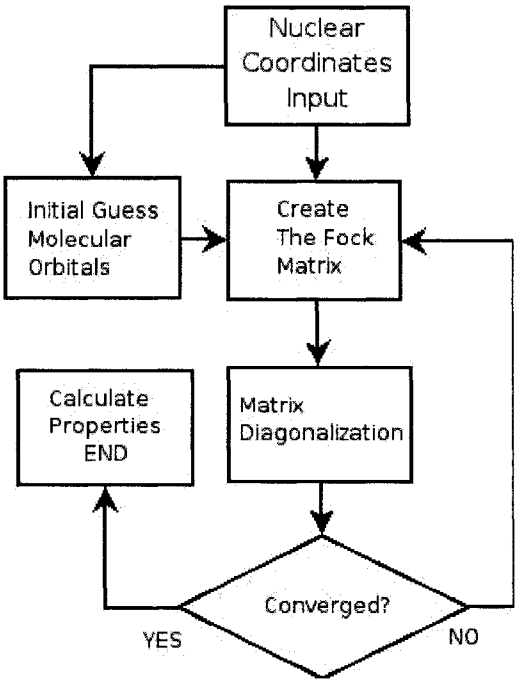

Figure 3.1 Self-Consistent-Field (SCF) schematic flow chart.

The nuclear coordinates used as input an be obtained using a molecular modeling software, that uses fast molecular dynamics algorithm and semi-empirical approach to create a starting point for the molecular geometry. The Fock matrix is an approximation of the real Hamiltonian operator of the molecular system under study. This matrix uses certain set of basis vectors called the "basis". SCF method method is a quite general approach to obtain *eigenvectors* that minimize the total energy of the system for a given molecular geometry (Levine, 1999a).

The HF methodology is based on the assumption that a single Slater determinant can represent the whole N-body wavefunction of the system under study. Then, the variational calculus will produce a set of N differential equations to be solved.

Despite the good accuracy that HF methodology offers, an important drawback is present; since the Fock matrix is a one electron operator, the electron correlation (dynamical electron-electron interactions) energy is not included, while the electron-electron repulsion is considered only as average. Therefore, the calculated total energy of the system is the so-called "Hartree-Fock limit" which is always greater (like in any variational method) than the real energy of the system.

In trying to solve the electronic correlation issue, P. Hohenberg and W. Kohn presented to the scientific community their seminal paper on "Inhomogeneous electron gas" theory which contains a demonstration that an electron gas interacting with any external potential $\hat{V}(\overrightarrow{r})_{ext}$ will have an universal density functional $F[n(\overrightarrow{r})]$ that is independent of $\hat{V}(\overrightarrow{r})_{ext}$, and for which the its minimum corresponds to the ground state energy of $\hat{V}(\overrightarrow{r})_{ext}$ (Hohenberg and Kohn, 1964). They also developed an exact formal variational for the ground state energy. Afterwards, in 1965, W. Kohn and J. Sham presented a set of one electron self-consistent equations (Kohn and Sham, 1965) that could be used to compute the ground state energy of inhomogeneous system of electrons that interact with an external potential.

Kohn and Sham rewrite the Hamiltonian operator (equation 3.11) to give the following monoelectronic equation:

$$\left(-\frac{1}{2}\nabla^2 + \hat{V}_{eff}(\overrightarrow{r})\right)\psi_v(\overrightarrow{r}) = E_v\psi_v(\overrightarrow{r}) \tag{3.11}$$

where $v = 1, 2, 3 \ldots$N represents the N particles, and replacing the potential for an effective potential ($\hat{V}_{eff}(\overrightarrow{r})$) that is written as:

$$\hat{V}_{eff}(\overrightarrow{r}) = v(\overrightarrow{r}) + \int \frac{n(\overrightarrow{r'})}{|r - r'|}dr' + \frac{\delta E_{xc}[\rho(\overrightarrow{r})]}{\delta\rho(\overrightarrow{r})} \tag{3.12}$$

where the first term is called the external potential, the second term describes

Coulomb repulsion between electrons, and the third term is exchange-correlation potential that includes all the particles interactions. $\rho(\overrightarrow{r})$ is defined as:

$$\rho(\overrightarrow{r}) = \sum_{n=1}^{N} \psi_n^*(\overrightarrow{r})\psi_n(\overrightarrow{r}) \tag{3.13}$$

3.2 Hybrid functionals

Hybrids functional are "mixtures" between exact HF exchange and the exchange and correlation of DFT. The first effort belongs to Lee C., Yang W., and Parr R. who developed a energy formula that is a functional of the electron density (Lee et al., 1988), followed by several contributions from Becke (Becke, 1988; Becke, 1992a; Becke, 1992b; Becke, 1993; Becke, 1996; Becke, 1997). Various approaches exist to calculate the exchange and correlation energy terms in DFT methods. These approaches differ in using either only the electron density, which are called Local Density Approximation (LDA) or the electron density as well as its gradients called gradient corrected methods or Generalized Gradient Approximation (GGA).

3.2.1 B3LYP functional

The B3LYP is an hybrid approach to evaluate the exchange and the correlation energies, that involves an empirical mixture of energy evaluated from DFT: Local Density Approximation (LDA) and Generalized Gradient Approximation (GGA) with the exact exchange energy obtained from Hartree-Fock. The name B3LYP stands for **B**ecke **3** (the number of empirical parameters used) **L**ee **Y**an **P**arr energy functional which is defined as (Becke, 1997),

$$E_{xc}^{B3LYP} = E_{xc}^{LDA} + a_o(E_x^{HF} - E_x^{LDA}) + a_x(E_x^{GGA} + E_x^{LDA}) + a_c(E_c^{GGA} - E_c^{LDA}) \quad (3.14)$$

where the energies in the equations are: x=exchange, c=correlation, HF= Hartree-Fock, LDA=Local Density Approximation, GGA=Generalized Gradient Approximation. a_o, a_x and a_c are the three empirical parameters that have been obtained through fitting the parameters to a set of thermochemical data.

3.3 Basis sets

Basis sets are mathematical functions that can be used to represent atomic orbitals. There are different types of basis sets available but in this work, we only use the Gaussian type. One Gaussian function could be used to describe atomic orbitals, therefore by making linear combinations of some of them, one can represent a molecular orbital. Thus, by using linear combination of Gaussian functions will give another Gaussian function as a result, that is a representation of the molecular orbital. Basis sets are often tested on a diatomic molecules for which an appropriate electronic state will reproduce the diatomic molecular electronic structure, bond length, bonding energy of experimental data.

3.3.1 The 6-311G** basis set

The Gaussian basis set used (for non metallic atoms) in this work was the 6-311G** (Krishnan et al., 1980) which is often referred as "full basis set". It is constructed using 6 Gaussian functions to describe each orbital in the core of the atom. Valence orbitals are constructed using 3 basis functions each. The first is a linear combi-

nation of 3 primitive Gaussian, the second and third use one Gaussian to describe the valence orbitals. The double star (**) refers to two different polarization functions (Gaussian functions), the first one to add p orbital functions to the hydrogen atoms, and the second to add d orbital functions to carbon atoms and f functions to the metallic atoms. Polarization functions are used to add an extra flexibility to molecular orbitals. For example, atoms bonded to hydrogen should have a certain degree of deformation of its spherical symmetry naturally produced by the bond itself.

3.4 The pseudopotential SDD

Pseudopotentials are mathematical functions that can represent the potential produced by the core electrons and the nucleus of certain atom in a molecule. The external electrons also known as the "valence electrons" are "immersed" in this potential created by the nucleus and the internal or core electrons. These valence electrons are explicitly treated during the computation, thus reducing the computational effort considerably. Pseudopotentials are specially useful when the system under study contains heavy atoms with a large number of electrons. For the metallic atoms (Pd, Pt and Ni) we have used the pseudopotential SDD (Stuttgart-Dresden) that have been developed since 1987 by different groups. (Fuentealba et al., 1983; Dolg et al., 1987; Igel et al., 1988; Andrae et al., 1990; Bergner et al., 1993; Figgen et al., 2005; Lim et al., 2005). We choose this pseudopotential because it contains the definition of a large number of atoms (from H trough Rn) including the selected metallic atoms. More importantly, calculations performed on a metallic diatomic molecule, give results that describes molecular properties with a good accuracy.

3.5 Software

In this research project, we have used the software Gaussian 03 (Frisch et al., 2004) that is the last version of this commercial code that has been originally developed by J. Pople. Results produced with Gaussian software are widely accepted by the scientific community due to its multiple capabilities implemented, and its large use by scientist all around the world. Gaussian contains a "molecular constructor" which was used to create all the input files used in our computations.

Once the wavefunction is known, many molecular properties can be evaluated using first principles procedures (Foresman and Frisch, 1996a). For example, the following properties of atoms and/or molecules can be obtained:

- Total molecular energy
- Geometry optimization
- Vibrational analysis
  - Raman, IR, NMR spectra
- Population analysis: Mulliken charge distribution
- Bond order index.

In our case, we have performed geometry optimizations, charge transfer and bond order computations.

3.5.1 Geometry optimization

The purpose of geometry optimizations is to locate the minimal energy based on the molecular geometry. This is translated into "try to find a stationary point" or a point on the potential energy surface where the forces are zero. The potential energy surface is just a mathematical abstraction which correlates one particular molecular structure and its corresponding energy. The optimization steps can be summarized as follows:

- Initial guess geometry.
- Solve SCF equations (3.6) and (3.7).
- Estimates the total energy gradient from the given geometry.
- Compute the total energy equation (3.5).
- Displace nuclear coordinates into the direction that minimizes the total energy (negative gradient).

This iterative process continues until the variation of the total energy from a step to another is lower than a convergence criterion. The algorithm used to achieve the optimized geometry is known as "Berny optimization algorithm" (Peng et al., 1996) with a convergence criterion of 1 x 10^{-6}. For the variation of energy, charge density and gradient from an iteration to the next.

3.5.2 Charge transfer

The charge transfer is the difference between the charge of a pyrene molecule before and after functionalization. The net charge are obtained from standard Mulliken

analysis.(Foresman and Frisch, 1996b) In this method, negative charges are assigned to the most electronegative atoms, and then is compensated by positives charges depending upon the electronegativity of each other atoms present in the molecule.

3.5.3 Bond order

According to Wiberg (Wiberg, 1968), a bond order index is a "measure" of the number of bonds between atoms in a molecular system. The bond order index (B) between atom "A" and atom "B" (B_{AB}) can be written:

$$B_{AB} = \sum_{\lambda \in A} \sum_{\sigma \in B} P^2_{\lambda\sigma} \tag{3.15}$$

where $P^2_{\lambda\sigma}$ is the density matrix of the basis function λ and σ centred on atom A and B, respectively. This matrix represents the total electron density in the region where the atomic orbitals overlap with each other (Atkins and Friedman, 1997).

We use the Wiberg bond order index to verify the changes in bonding in the pyrene molecule. It is important to verify if the aromaticity is broken after the functionalization, since CNTs are highly aromatic systems, our model must represent as close as possible all the aspects. Therefore, if the functionalization of pyrene disrupt its aromatic character our model is not longer valid as a solid CNTs representation. Also, bond order analysis will allow us to verify how strong will be the bond between the metallic particle and the functionalization group (Levine, 1999b), once the stabilization computations are performed.

3.6 From pyrene to multi-walled carbon nanotubes

Since multi-walled carbon nanotubes (MWCNT) are molecules that may easily contain multi-millions of atoms, (see figure 3.2) performing DFT calculations on such systems are impractical. Hence, we need to use a simpler model that mimics the nanotube properties and that would allow us to investigate many functionalization schemes within a reasonable time.

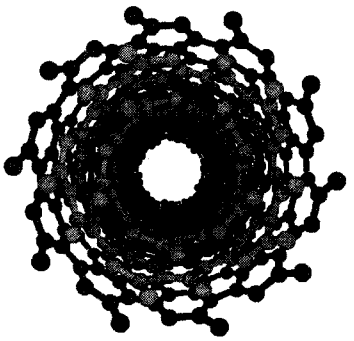

Figure 3.2 Schematic representation of a MWCNT.

If we consider a single concentric tube from the figure 3.2, then we have single-walled carbon nanotube (SWCNT). This system is still too large to be treated with DFT calculations. A more drastic solution is to consider a pyrene molecule as a representative unit of a nanotube (See Figure 3.3).

By this choice, we are making a few important assumptions. First we consider that internal walls of a SWCNT do not offer a suitable place for reactions to take place. Second, we do not consider long range interactions in the reactivity and we limit our chemical investigation to local properties. However, a model of the size of pyrene will allow us to investigate several functionalization scheme in a reasonable time. Since the central carbon atoms of the molecule have a similar coordination (3) to carbon in carbon nanotubes, the reactivity of those carbon atoms should be

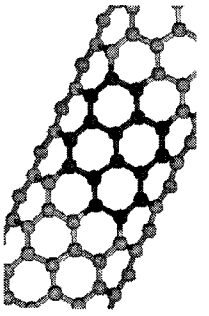

Figure 3.3 Schematic representation of a SWCNT as a succession of pyrene molecule (dark).

close to carbon atoms in carbon nanotubes.

CHAPTER 4

RESULTS ON THE FUNCTIONALIZATION OF PYRENE

In this chapter, we present our theoretical results on pyrene functionalization. The functional groups considered during the course of this research will be also presented. First, it is worth to mention and to describe, at least partially, some basic concepts often used in chemistry (Wade, 1999; Pine, 1980). This should help to understand different aspects of the results, like the direction of the charge flow due to formal charges, and the deformation of pyrene due to the steric effects induced by the presence of the functional groups.

4.1 Structural effects

Certain kinds of structural effects present during the evolution of a chemical reaction could have a significant impact on the final molecular structure. They are classified in three major groups:

- Inductive effect
- Resonance effect
- Steric effect

4.1.1 Inductive effect

This effect refers to the polarization of bonds in a molecule induced by the presence of an adjacent group or atom with a distinct electronegativity. Because of this difference, electrons will be attracted to atoms that have higher electronegativity, thus producing an electric dipole. This enables the transmission of charge through a chain of atoms by electrostatic induction, placing pseudo charges over the atoms that conforms the molecule. We see in Figure 4.1 the formal charges on the fluoromethane molecule as an illustrative example.

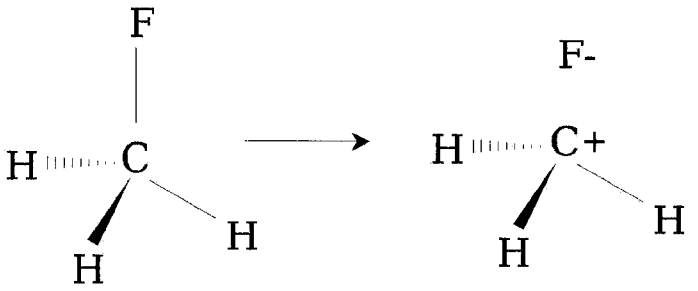

Figure 4.1 Fluoromethane as an example of formal charges example.

4.1.2 Resonance effect

The interaction among electrons in conjugated bonds is probably one of the most important structural effect. Figure 4.2 [1] shows the resonance of π electrons in benzene as an illustrative example. In order to "build" a benzene molecule, we may use cyclohexane as starting point. We then remove two hydrogen atoms and create a double bond between carbon atoms, a reaction known as dehydrogenation. This specie called cyclohexene has a formation energy of -120 kJ/mol. Afterward, we add

[1] taken from: http://people.uis.edu/gtram1/organic/aromatics/benzene.htm

a second double bond to form 1,3-cyclohexadiene. We expect an amount of energy around -240 kJ/mol, but a value of -231 kJ/mol is experimentally measured. It is then 9 kJ/mol more stable. After the third dehydrogenation, benzene turns out to be 152 kJ/mol more stable than the theoretical prediction. This energy stabilization is known as resonance, and it is observed in molecules that have conjugated π systems, or molecules with sp^2 hybrid atoms, and therefore allowing π electrons to flow between these orbitals. Such electron delocalization among the carbon atoms of the molecule, makes benzene more stable than what is theoretically expected.

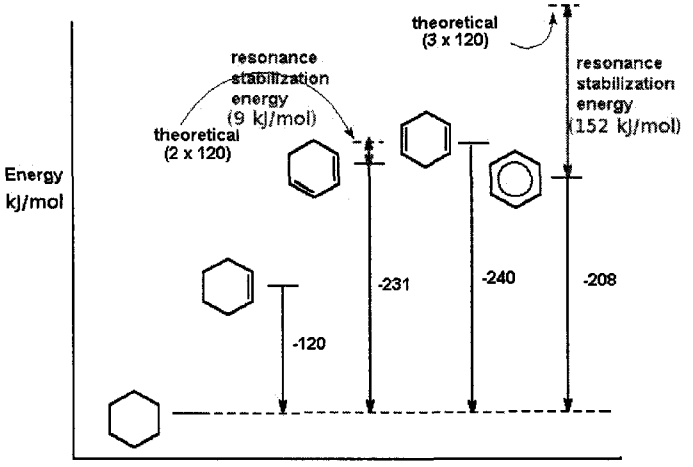

Figure 4.2 Building up a benzene from a cyclohexane, an example of resonance effect.

4.1.3 Steric effect

This effect represents the influence of the spatial configuration of a reactant upon the rate, the nature, and the extent of a chemical reaction. We see in figure 4.3 a representation of a tri-tert-butyl-methane as an example of a molecule with very strong steric effects between voluminous tert-butyl groups (figure 4.3-B). In such molecular arrangement, these large groups tend to repeal each other to minimize repulsion energy associated to the proximity of the different nuclei. For illustration

purposes, we present also a bond representation (figure 4.3-A) of the molecule. We have also pointed in 4.3-B some of the zones where the groups are very close to each other. A detailed inspection of the model should reveal that, in fact, steric effects are present in the whole molecule.

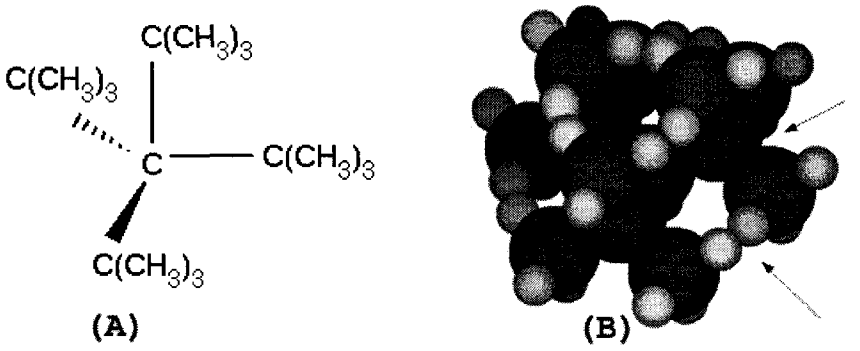

Figure 4.3 Schematic representation of tri-tert-butyl-methane (A) bond representation, (B) space filling representation.

In summary, these structural effects should allow us to classify the functional groups that will be considered during the course of this research. We will split the six functional groups considered in two sub-groups that depend upon their abilities to donate or to withdraw charge.

4.2 Functional groups

4.2.1 Electron attractors

Electron attractors can be defined as molecular systems, that due to their electronic properties, are able to attract or withdraw electron density from another molecule. If an electron attractor is used to functionalize pyrene, then we may expect that some electronic density towards the functionalization group will be transferred.

The selected molecules for their electron attracting properties are CN, COOH, and $Si(OH)_3$. A ball and stick representation of these compounds is given on Figure 4.4.

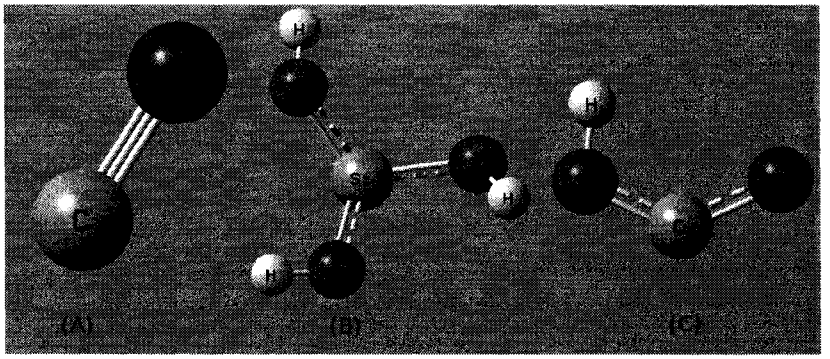

Figure 4.4 Selected electron attractors: (A) CN, (B) $Si(OH)_3$, (C) COOH.

We may see that a positive formal charge could be placed on C atom in CN molecule (A). Supported by an inductive effect a positive charge would also appear on C atom in the COOH molecule (C). Inductive effect could also be used to explain the positive charge on the Si atom (B). In addition, Si atom in $Si(OH)_3$ molecule (B) presents steric effect due to the numerous OH groups. The presence of formal positive charge on atoms that are bonded to pyrene suggest a charge transfer from pyrene to the functional group.

4.2.2 Electron donors

In contrast, electron donors are molecular systems that are able to give or donate electron density. The following groups are used in the present study: NH_2, SiH_3, and OH. (See Figure 4.5).

Due to a difference in electronegativities, a formal negative charge could be assigned to N atom in NH_2 (A), to Si atom in SiH_3 (B), and to O atom in OH (C). Since these functional groups establish bonds with pyrene through the negatively charged atom, we may then expect some electron density to be transferred to pyrene upon

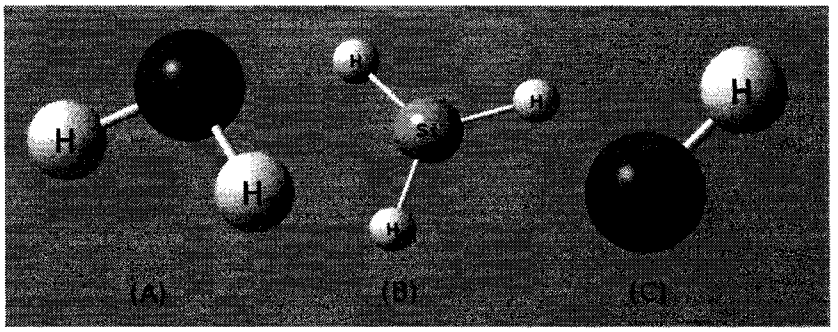

Figure 4.5 Selected Electron Donors (A) NH_2, (B) SiH_3, (C) OH.

its functionalization. We can also note that steric effect is also present to a certain degree in SiH_3.

4.3 Pyrene functionalization

Two types of functionalization scheme of pyrene have been considered. The *cis* where functional groups are in the same side of pyrene and the *trans* where the groups are located in opposite sides of the molecular plane. All models are built and optimized as described in Chapter III. We have obtained the bonding energies, charge distributions, bonding characters, and the structural parameters. In order to avoid the presence of dangling bonds on pyrene, *cis* and *trans* isomers were studied using two identical functional groups (homofunctional), or using one group and one hydrogen atom (heterofunctional). In Figure 4.6, *cis* and *trans* homofunctional isomers with CN groups is used for illustration. We have decided to consider the *trans* isomer in order to establish a comparison between both isomers stability.

Figure 4.7 shows the *cis* and *trans* isomers containing one functional group and one hydrogen atom (heterofunctional), and where the functional group used is NH_2.

Pyrene is a graphite-like molecule, hence is flat. We choose the set of four carbon

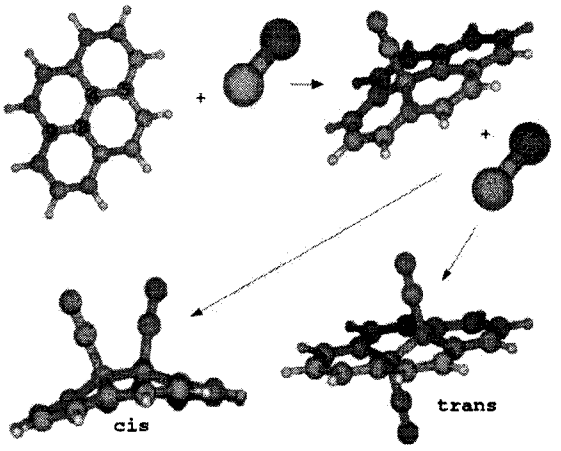

Figure 4.6 Homofunctional *cis* and *trans* isomers of CN on pyrene.

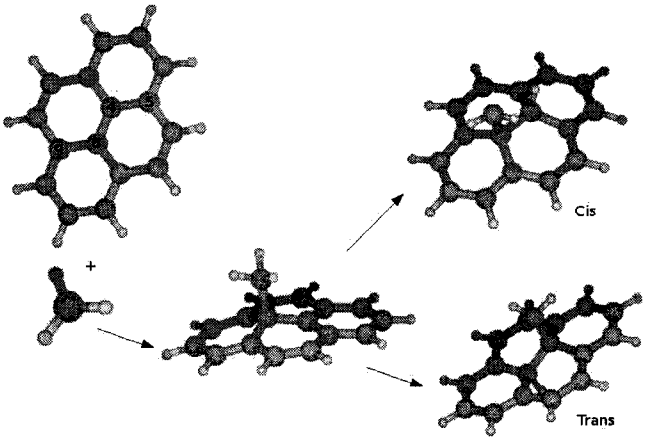

Figure 4.7 Heterofunctional *cis* and *trans* isomers of NH_2 on pyrene.

atoms in the molecule that are labeled 4, 5, 8, 9 in Figure 4.8, form a 180° dihedral angle. Variation of this dihedral angle will be considered a measure of the molecular deformation after functionalization.

The functionalization was only considered at the sites labeled 4 and 8 in figure 4.8. They form sp^2 bonds with their nearest neighbors just like carbon atoms in a graphene sheet or in a CNT. All the dihedral angles presented in this work were determined from these four selected carbon atoms labeled 4, 5, 8 and 9.

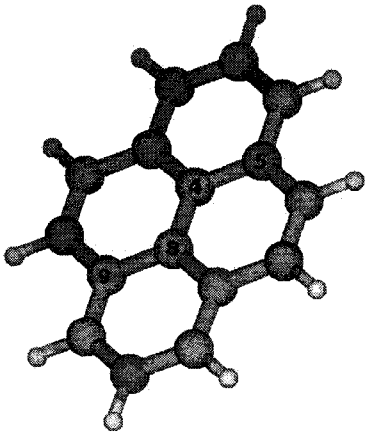

Figure 4.8 Schematic representation of pyrene showing the central carbon atoms (4 and 8).

As mentioned before, all carbon atoms are hybridized sp^2. Thus, as soon as a functionalization is performed, carbon atoms involved in the bonding would change their hybridization from sp^2 to sp^3 in order to form a bond with the functional group. Therefore, pyrene structure will be disrupted and significant deformations should occur within the molecule.The magnitude of deformation ($\%_{Def}$) of each compound is evaluated using the following equation,

$$\%_{Def} = \left[100 - \frac{dihedral * 100}{180}\right] \tag{4.1}$$

where dihedral is the calculated dihedral angle (°) between carbon atoms 4, 5, 8, 9. The deformation energy (E_{def}) of each compound is,

$$E_{def} = E_{Def.py} - E_{(flat)} \tag{4.2}$$

where $E_{Def.py}$ is the energy of the deformed pyrene but without the functional groups, preserving the current status of the bonds in the molecule. (see figure

4.9-B) and E_{flat} is the energy of the flat pyrene molecule (fig. 4.9-A). An example of deformed pyrene is shown in Figure 4.9.

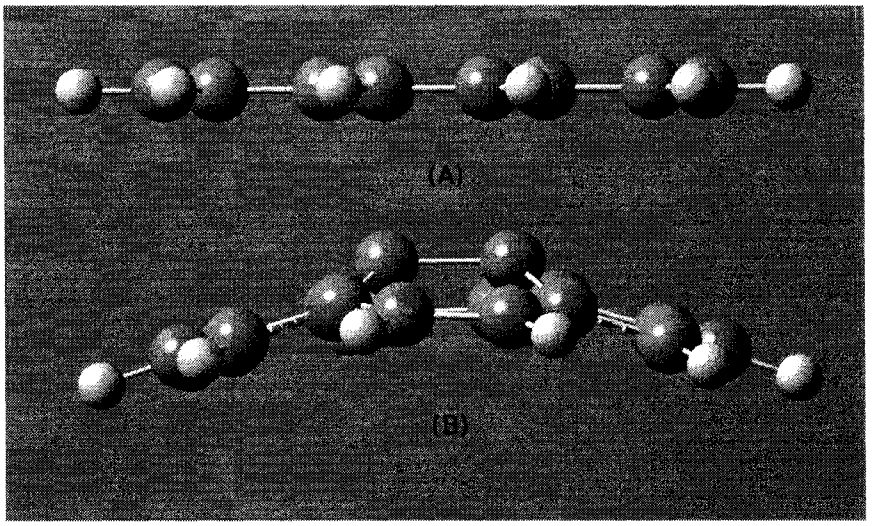

Figure 4.9 Side view of pyrene (A) before functionalization (B) after functionalization (functional groups were removed).

We will use the bonding energy of functional groups to pyrene to classify the bond strength of each functional groups. The homofunctional bonding energy (BE_{homo}) is computed using:

$$BE_{homo} = (E_{def} + 2 * E_{group}) - E_{funct} \tag{4.3}$$

The energy (BE_{homo}) is the amount of energy needed to break the bond between the two functional groups and pyrene. The heterofunctional bonding energy (BE_{hetero}) which the energy required to break both functional group and hydrogen bond with pyrene, is calculated using:

$$BE_{hetero} = (E_{def} + E_{group} + E_H) - E_{funct} \tag{4.4}$$

where E_{def} is the total energy of the deformed pyrene, E_{group} is the total energy

of the functional group, the E_{funct} is the total energy of the functionalized pyrene, and finally E_H represents hydrogen atom total energy. Since we are considering the energy of deformed pyrene, this bonding energy should be considered as the minimal energy needed to break bonds between the functional groups and pyrene. To calculate the functional group total energy, a model of the functional group is constructed, afterwards an optimization is performed. For the hydrogen since is an atom the energy is estimated performing a single point energy calculation.

Finally, the transferred charge (TC) is calculated with:

$$TC = Ch_{pyrene} - Ch_{funct} \tag{4.5}$$

where Ch_{pyrene} is the Mulliken population on C4 and C8 of pyrene, and Ch_{funct} is the population on C4 and C8 of pyrene after the functionalization.

4.4 Results of the homofunctionalization

Using the techniques described in Chapter III, the *cis* and *trans* complexes were built, and then fully optimized. Here, we present the electronic structure properties obtained, such as the bonding energy, the charge transfer and bond orders of the optimized complexes. We recall that the optimization algorithm have a convergence criterion of $1x10^{-6}$ which represents our level of uncertainty.

4.4.1 Bonding energy

In Table 4.1, the calculated bonding energy of *cis* and *trans* isomers are presented. We observe that all *trans* complexes are little more stable than the *cis* ones, with the only exception of $Si(OH)_3$.

Table 4.1 Calculated bonding energies (eV) for *cis* and *trans* pyrene-R_2 complexes.

Character	Group (R)	*cis* pyrene-R_2	*trans* pyrene-R_2
Donor	-OH	4.65	4.73
	$-NH_2$	4.05	4.22
	$-SiH_3$	3.58	3.69
Attractor	-CN	6.63	6.88
	$-Si(OH)_3$	4.70	4.21
	-COOH	3.73	3.80

Table 4.2 Calculated dihedral angles, percentage and deformation energies after functionalization.

Character	Group	Dih. Angle (°)		Def. %		Def. energy (eV)	
		Cis	Trans	Cis	Trans	Cis	Trans
Donor	$-NH_2$	131.7	179.7	26.8	0.7	3.29	2.97
	$-SiH_3$	134.1	180.0	25.5	0.0	3.21	2.81
	-OH	134.6	179.6	25.2	0.2	2.99	2.72
Attractor	$-Si(OH)_3$	127.5	180.0	29.2	0.0	3.64	2.55
	-CN	130.5	178.9	27.5	0.6	3.35	2.90
	-COOH	131.4	180.0	27.0	0.0	3.29	2.93

Table 4.2 shows the calculated dihedral angles, percentage and energy deformation of pyrene molecule after functionalization. The % of deformation of *trans* complexes appears very weak because the deformation induced is symmetric with respect to central carbon atoms, thus calculated dihedral angles are close to 180°. Nevertheless, the deformation energy for *trans* complexes is in the same range than *cis* complexes. In contrast, deformations in *cis* complexes gives some curvature to the pyrene, since the presence of both functional groups in the plane, tends to be separate from each other producing a curvature on pyrene. See figure 4.10 for an illustrative example of both types of deformations.

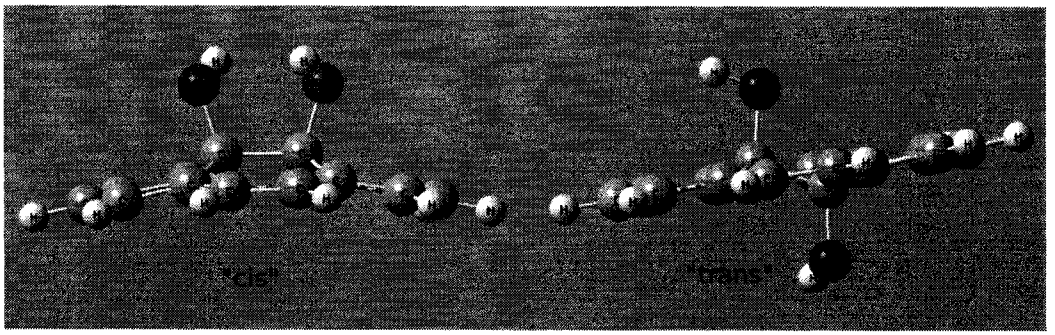

Figure 4.10 Side view of *cis*-pyreneOH and *trans*-pyreneOH.

4.4.2 Charge transfer

The top of the table 4.3 gives the net charge transfer for donors groups, while the net charge transfer for attractor groups is given at the botton. Negative sign means a gain of negative charge (electrons) while a positive sign represents a loss of negative charge from pyrene.

Table 4.3 Calculated net charge transfer (TC) of the homofunctionalized pyrene molecule.

Character	Cis and Trans	C4	C8
Donor	pyrene-NH_2	-0.14	-0.13
	pyrene-OH	-0.27	-0.27
	pyrene-SiH_3	-0.40	-0.40
Attractor	pyrene-$Si(OH)_3$	0.47	0.47
	pyrene-COOH	0.14	0.14
	pyrene-CN	0.13	0.13

Table 4.3 clearly reveals a significant charge transfer from the donor groups to C4 and C8 of pyrene molecule. In contrast, the attractor groups withdraw some charge from them since atoms 4 and 8 have now a positive value.

4.4.3 Bond order and structural data

Although the absolute value of bond order remains only qualitative, its variation can be used to discuss the nature of the bonding. Bond order analysis of pyrene shows that every carbon-carbon bond has a value of 1.4, thus confirming the aromatic character of the molecule. After the functionalization some of these values change (shown on Figure 4.11). The calculated bond order is nearly 1.4 for every carbon-carbon bond except on the central carbons where it decreases to 1.0, therefore having a single bond between C4 (or C8) and the functional group. This decrease is clearly due to the functionalization. This trend is similarly observed on *cis* and *trans* complexes considered. The calculated bond orders for the bond formed are reported in Table 4.4.

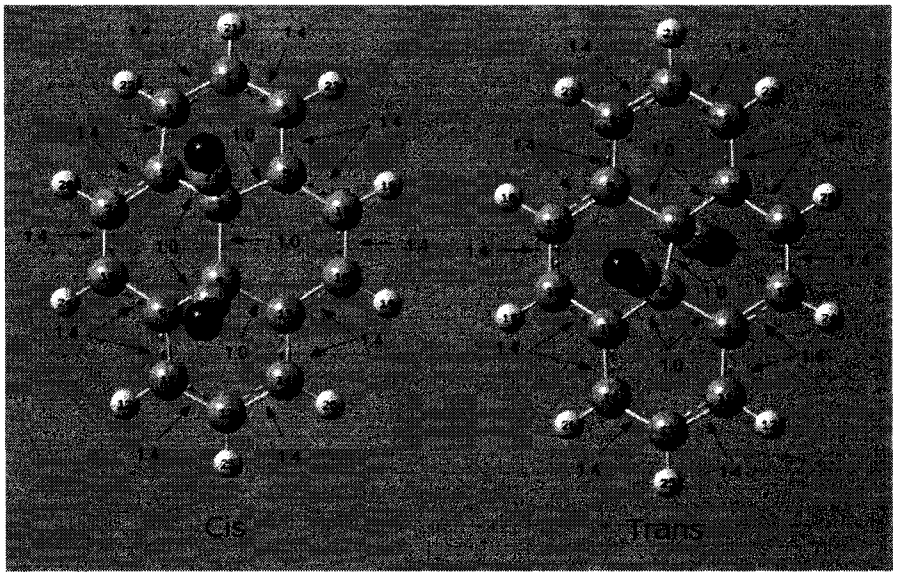

Figure 4.11 Calculated bond order for *cis* and *trans* complexes. (using CN as functional group)

We see in the Figure 4.11 that the aromaticity of pyrene is broken in the central region due to the functionalization. Other carbon-carbon bonds present invariably a value of 1.4, which is according to the Wiberg theory, a double bond in an

aromatic system.

Table 4.4 Calculated bond order between carbon and functional group.

Character	Group	*Cis* and *Trans*	
		C4-Group	C8-Group
Donor	$-NH_2$	0.97	0.97
	-OH	0.88	0.89
	$-SiH_3$	0.69	0.68
Attractor	-CN	0.99	0.98
	-COOH	0.89	0.90
	$-Si(OH)_3$	0.61	0.60

We can also see in Table 4.4 that voluminous groups like $Si(OH)_3$ present weaker bond orders than smaller groups like CN. This behavior is also observed in both donors and attractors. We can also observe a tendency of decreasing bond order when the magnitude of charge transfer is increased.

4.5 Results of the heterofunctionalization

In this section, we will present the results on heterofunctionalization (see Figure 4.7). We want to explore the influence of a different group (hydrogen in this case) on the values of bonding energies, bond orders, or charge transfer of the selected functional group.

4.5.1 Bonding energy

In Table 4.5, the calculated *cis* and *trans* pyreneH-R complexes bonding energies are summarized. We observe that bonding energies are higher for the heterofunctionalization than for homofunctionalization. As expected, *trans* complexes are

more stable than *cis*. This is because the *trans* isomers have the functional groups on opposite sides of the molecular plane of pyrene which leads to a decrease of the steric interactions between them.

Table 4.5 Calculated bonding energy of heterofunctionalized pyrene.

Character	Group (R)	*cis* pyreneH-R (eV)	*trans* pyreneH-R (eV)
Donor	-OH	4.80	5.19
	$-NH_2$	4.54	4.92
	$-SiH_3$	4.46	4.69
Attractor	-CN	6.04	6.30
	$-Si(OH)_3$	4.67	4.95
	-COOH	4.63	4.78

Since we have considered only the case of homolytic bond breaking, meaning the breaking of the two bonds simultaneously, the bonding energy obtained is the energy needed to break individual C-R and C-H bonds combined. In Table 4.6 we see calculated dihedral angles, % and energy deformation of *cis* and *trans* complexes. We observe that deformations of the *cis* heterofunctionalized complexes are in general lower than the observed in the *cis* homofunctionalized. This is simply due to the fact that deformation exerted on pyrene is not symmetric with R + H groups, therefore the perturbation it is not equally distributed. Hydrogen will induce smaller deformations on its side if compared with the induced by the functional group. For the same reason *trans* heterofunctional complexes display higher deformations than their homofunctional counterparts.

4.5.2 Charge transfer

In Table 4.7, we summarized the different calculated charge transfer for *cis* and *trans* pyreneH-group complexes. The type of bonds formed in the *cis* and *trans* complexes are practically the same.

Table 4.6 Calculated dihedral angles, % and deformation energies of heterofunctionalized pyrene.

Character	Group	Dih. Angle (°)		Def. %		Def. energy (eV)	
		Cis	Trans	Cis	Trans	Cis	Trans
Donors	-OH	134.1	176.0	25.5	2.2	2.83	2.53
	$-SiH_3$	136.1	178.6	24.4	0.8	2.80	2.52
	$-NH_2$	135.3	174.9	24.8	2.9	2.53	2.66
Attractors	$-Si(OH)_3$	134.9	175.7	25.1	2.4	2.73	2.65
	-COOH	134.4	177.7	25.4	1.3	2.67	2.67
	-CN	136.7	176.3	24.1	2.1	2.35	2.68

Table 4.7 Charge transfer for the heterofunctionalized pyrene systems.

Character	*cis* and *trans*	C4-R	C8-H
Donors	$-NH_2$	0.26	-0.15
	-OH	0.27	-0.30
	$-SiH_3$	0.23	-0.41
Attractors	$-Si(OH)_3$	0.48	0.22
	-COOH	0.23	0.15
	-CN	0.15	0.21

Due to the difference in electronegativity between carbon and hydrogen atoms, we have expected to have some charge transfer from hydrogen to C8, but this trend was observed only for donors. C4 with donors does not gained any charge from the group. For the attractors, we clearly see a net charge being transferred from the pyrene to the functional group.

4.5.3 Bond order and structural data

If we compare the homofunctionalization (table 4.4), we observed similar results for both *cis* and *trans* complexes. Calculated bond order of carbon-group and carbon-hydrogen bonds are summarized in Table 4.8

Table 4.8 Calculated bond order for carbon to functional group bonding.

Character	Group (R)	*cis*		*trans*	
		C4-R	C8-H	C4-R	C8-H
Donors	$-NH_2$	0.94	0.83	0.96	0.84
	-OH	0.85	0.81	0.88	0.83
	$-SiH_3$	0.68	0.87	0.69	0.85
Attractors	-CN	0.99	0.85	0.98	0.84
	-COOH	0.90	0.85	0.90	0.84
	$-Si(OH)_3$	0.60	0.87	0.61	0.85

We see that bond orders of C-R do not show large differences between homo and heterofunctionalized complexes. We also see that voluminous groups such as $Si(OH)_3$ have lower bond orders than smaller functional groups like CN. For hydrogen as functional group we observe a value that corresponds to a singe bond.

4.6 Summary

We have presented results on pyrene functionalization using two schemes defined as homo and heterofunctional where for both types of isomers *cis* and *trans* were studied. We have seen that the charge is transferred as a function of the nature of the functional group used, donors transfer some charge to the C4 and C8 of pyrene while attractor whitdrawn some charge. The results of Wiberg bond order indexes and the structural data of the functionalized molecules of pyrene were also presented. We observed that the bond order is directly related to the bonding energy of the groups, but is not strongly influenced by the type of functionalization (homo or heterofunctionalization). In the next chapter we will introduce the stabilization of metal particles over these functionalized pyrene compounds.

CHAPTER 5

RESULTS ON THE STABILIZATION OF METAL PARTICLES

In the previous chapter, we have explored the functionalization of the pyrene molecule using six different anchoring groups. In this chapter, we will present how these functional groups can stabilize metallic particles on pyrene. Using functionalized pyrene molecules as a starting point, we have considered the bonding of metallic particles directly to the functional groups. In this serie of computations, we allowed the metallic particle, the functional groups, and the central carbon atoms to relax, while the rest of the system was kept frozen. Since most of the structural variations happens in the vicinity of the chemical perturbation, the structural changes in the surroundings of central carbon atoms will be minimized. We have performed the calculations on three different isoelectronic metals Pt, Ni and Pd. All the selected metals belong to the group 10 of the periodic table. They have ten valence electrons that are distributed among d and s orbitals. Their atomic ground state configurations are:

1. Platinum (Pt) $[Xe]4f^{14}5d^{9}6s^{1}$
2. Palladium (Pd) $[Kr]4d^{10}$
3. Nickel (Ni) $[Ar]3d^{8}4s^{2}$

To evaluate the stabilization of the metal, we will use the energy required to dissociate a single atom (or groups of atoms) from the complex. Results of the bonding energies are reported on complexes with a single metal atom and also with a metal dimer bonded to the functional groups. As a reference, we will consider the "bridge"

bonding where a metal atom is directly bonded to pyrene without functional groups. This will allow us to directly evaluate the effect of functional groups on the stabilization of the metal particle. Bridge bonding represents the current state of a real catalyst in fuel cells, since platinum particles are deposited directly over carbon black.

5.1 One metal atom systems

5.1.1 Bridge bond

As mentioned above, a bridge bond is made by bonding the metal atom directly to the pyrene molecule. A schematic representation of this type of bonding is shown in Figure 5.1. The metal atom is bonded directly to the central carbon atoms (labelled as C4 and C8) of pyrene. Results of the calculated bonding energies (BE), charge transfer (TC) and bond order (BO) are presented in the Table 5.1.

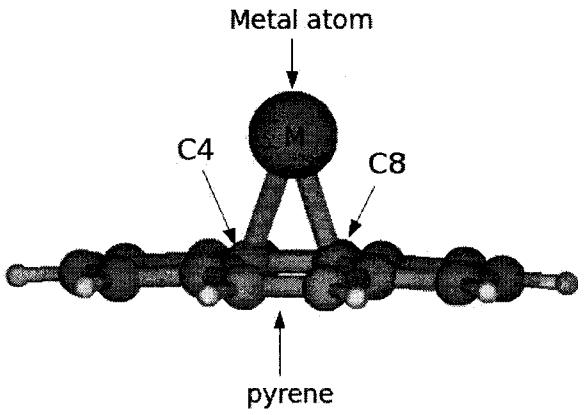

Figure 5.1 Schematic representation of a "bridge" bond on pyrene.

We see that metal atoms are more weakly bonded to pyrene than to functional groups. Small values of bonding energies may suggest that metallic particles can

move more easily on the surface of pyrene at higher temperatures. This result is consistent with the significant coalescence observed experimentally, as described in Chapter 1.

Table 5.1 Singlet state bonding energies, charge transfer, bond order and deformation for metallic bridge bond.

	B.E.	T.C.			Bond Order			Deformation		
M	(eV)	C4	C8	M	C4-M	C8-M	Total	Dih (°)	%	E. (eV)
Ni	1.29	-0.11	-0.11	0.37	0.29	0.29	0.98	163.9	9.0	0.31
Pt	1.28	-0.09	-0.09	0.16	0.25	0.25	0.97	169.3	6.0	0.16
Pd	0.56	-0.07	-0.07	0.20	0.12	0.12	0.53	170.6	5.2	0.11

Bond orders for metal-carbon (C4 and C8) bonds are small which means that a weak bond is formed. The total bond order takes into account all the interactions present between pyrene and the metal atom, and we obtain for Pt and Ni values that are close to one. Thus, a single bond is formed, which is consistent with the calculated bonding energy of 1.3 eV of Pt and Ni to pyrene. In contrast, palladium bonds very weakly to pyrene since both bonding energies and total bond order have low values. We also observe a small charge being transferred to central carbon atoms of pyrene, leaving a positive charge over the metal atoms.

Finally, we see also in the Table 5.1 that pyrene molecule is not importantly deformed with metal adsorption. Ni shows the highest degree of deformation and deformation energy, which are related to the higher bond order and bonding energy calculated. This is probably due to its electronic configuration ($[Ar]3d^84s^2$) it has 8 electrons located in d orbitals, that are more easily polarizable than Pd and Pt which shows a more closed "d" shell that mix less naturally with "sp" orbitals of pyrene.

5.1.2 Adsorption on functional groups

We will now present how the influence of functional group on the bonding energy, or in other words on the stabilization of the metal particles. In Figure 5.2, we show (in two examples) a schematic representation of a metal atom bonded via the functional group to pyrene in the *cis* configuration. Only the *cis* configuration was considered, since it represents the real model of a sidewall functionalization of carbon nanotube.

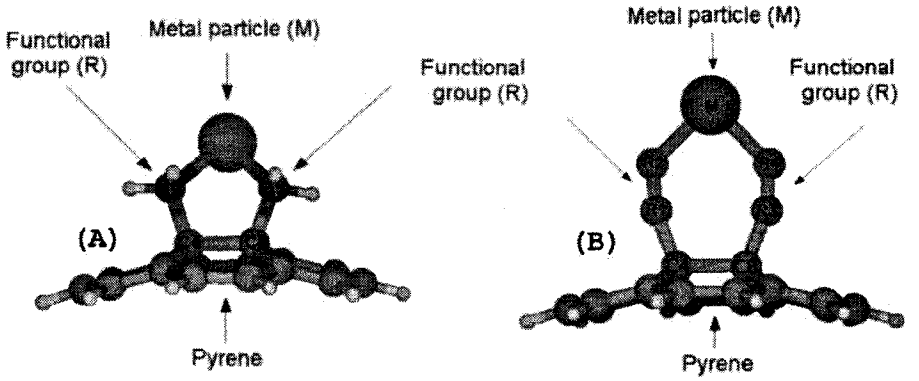

Figure 5.2 Two examples of one metal atom (M) bonded to pyrene via functional group (R). (A) *cis*-pyreneNH_2 (B) *cis*-pyreneCN.

We obtain higher values of bonding energies when functional groups are present than when the metal atom is directly bonded to pyrene. We also found significant variations among the different functional groups that depend on the donor or attractor character of the groups. We report in Table 5.2 the calculated bonding energies, charge transfer and the bond order.[1]

We observed that the calculated bonding energies with the selected donor molecules have low values, and suggest the formation of weak bonds. In contrast, the attractor groups display higher bonding energies which translate into stronger bonds. Table

[1]Where C stands for character, D for donor and A for attractor

Table 5.2 Bonding energies, charge transfer and bond orders for functionalized pyrene + one metallic atom.

C	Group	B.E. (eV)			T.C.			B.O.		
		Pt	Pd	Ni	Pt	Pd	Ni	Pt	Pd	Ni
D	NH_2	1.91	1.19	0.86	0.05	0.03	0.34	0.84	0.54	1.24
	SiH_3	1.11	0.69	0.12	0.07	0.11	0.20	0.80	0.56	0.97
	OH	0.97	0.53	0.08	0.00	0.27	0.46	0.49	0.26	1.04
A	$Si(OH)_3$	3.14	1.89	0.85	0.23	0.02	0.31	1.85	1.25	1.71
	COOH	3.03	1.70	0.51	0.49	0.45	0.67	1.88	1.29	1.67
	CN	2.06	1.29	1.54	0.33	0.27	0.46	1.40	0.94	1.48

5.2 also shown that there is some charge being extracted from the metallic atom, all of them appear with a positive value. No significant changes occurred for carbon atoms of the functionalized pyrene. The fluctuation of charge mainly occurred between the functional group and the metallic atom.

Total bond order values for metal-R bond are in the same range (for the donors) than the metal-pyrene bond previously showed in Table 5.1. High bond order values are more generally observed among the functional groups with attracting character, and they also have higher bonding energies values. The attractor groups for the specific case of platinum, we observe values close to 2. Such high bond order values are directly related to high bonding energy values, and suggest that metal particles are strongly stabilized by these functional groups.

We see in Table 5.3[2] that $Si(OH)_3$ group induces a stronger deformation of pyrene (32%), than any other functional group. It is also important to note that the deformation energies are larger for all the functional groups than the case of the metal atom directly bonded to pyrene (see table 5.1).

[2]Where C stands for character, D for donor and A for attractor

Table 5.3 Calculated dihedral angles, degree of deformation (%) and deformation energies (eV) of functionalized pyrene + one metal atom systems.

C	Metal →	Pt			Pd			Ni		
	Group ↓	Angle	%	D.E.	Angle	%	D.E.	Angle	%	D.E.
D	SiH_3	134.1	25.5	3.26	134.1	25.5	3.26	134.1	25.5	3.26
	NH_2	130.4	27.6	3.21	130.2	27.7	3.22	131.7	26.8	3.33
	OH	134.1	25.5	2.68	129.8	27.9	3.04	129.8	27.9	3.04
A	$Si(OH)_3$	122.4	32.0	3.49	122.4	31.8	3.47	122.4	32.0	3.49
	COOH	128.7	28.5	3.45	130.5	27.5	3.41	130.0	27.8	3.23
	CN	128.8	28.5	3.87	129.5	28.1	3.70	128.1	28.9	4.09

5.2 Two metal atoms systems

In Figure 5.3, we give a representation of this type of complex. In this configuration the metal dimer is bonded through one atom directly on the functional group. This model resembles the one metal particle model previously used, with the difference that a metal-metal bond is also present.

In Table 5.4, we summarized the calculated bonding energies for two metal atoms systems. As before, the functional groups, carbon atoms 8 and 4 and the metal dimer are allow to relax during geometry optimization. The distance between M1 and M2 was fixed to the values obtained for an isolated metal dimer.

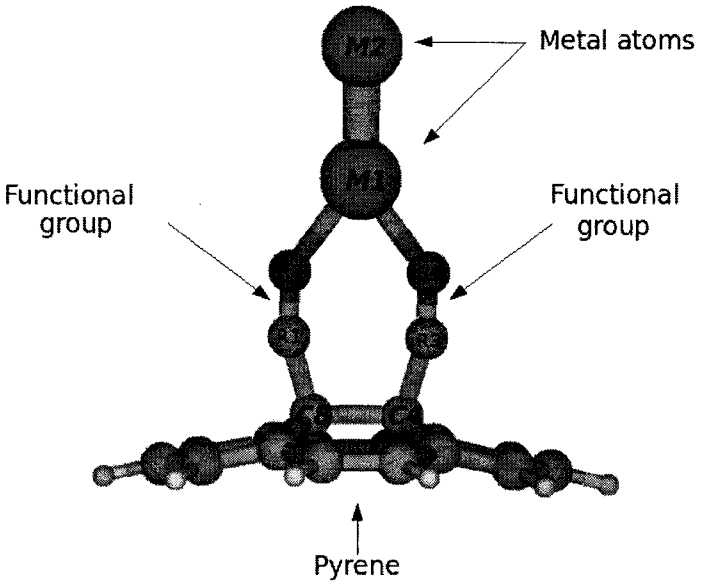

Figure 5.3 Schematic representation of two metallic atoms bonded to pyrene via functionalization groups, in *cis* configuration.

Table 5.4 Calculated bonding energies (eV) for functionalized pyrene + two metal atom systems.

Character	Group	Pt	Pd	Ni
Donor	NH_2	2.01	1.11	0.82
	SiH_3	1.16	0.52	0.15
	OH	0.85	0.51	0.02
Attractor	$Si(OH)_3$	3.37	1.76	0.73
	COOH	3.10	1.72	0.81
	CN	1.97	1.25	1.49

The bonding of metal to OH group gives weak bonding energies. NH_2 complex shows the highest bonding energy for the donor group, while CN gives the highest bonding energy for the attractor group.

On Table 5.5, we see some evidence of charge transfer between the functional group and the metal atoms. Nevertheless, while the pyrene molecule remains essentially uncharged after the metal particles adsorption. For SiH_3 and NH_2 complexes, some

charge transfer is observed from the functional group to the metal (M1). For the CN and $Si(OH)_3$ (attractor groups) a small amount of charge is transferred to Pt.

Table 5.5 Calculated charge transfer (TC) of functionalized pyrene + two metal atom systems.

Character	Group	Pt(1)	Pt(2)	Pd(1)	Pd(2)	Ni(1)	Ni(2)
Donor	SiH_3	-0.2	0.0	0.0	0.1	-0.1	0.1
	NH_2	-0.5	0.3	-0.3	0.3	-0.3	0.3
	OH	0.0	0.0	0.0	0.0	0.0	0.0
Attractor	$Si(OH)_3$	-0.1	-0.1	-0.1	0.2	0.0	0.0
	COOH	0.0	0.1	0.1	0.1	0.2	0.2
	CN	-0.4	0.4	0.1	0.0	0.1	0.1

In Table 5.6 we summarize the calculated total bond order for the M1 metal atom. As mentioned before M1 is the metal atom that interacts directly with the functional group, while the distance M1-M2 remains fixed during the optimization. The OH and $Si(OH)_3$ complexes showed small bond order values in relation to their low bonding energies. Nickel and palladium atoms have small bond order values with respect to the values calculated for platinum atoms.

Table 5.6 Total calculated bond order for two metal atoms systems.

Character	Group	Pt(1)	Pd(1)	Ni(1)
Donor	NH_2	2.28	1.90	0.42
	SiH_3	2.18	0.73	0.30
	OH	0.56	0.19	0.57
Attractor	CN	1.95	0.75	1.00
	COOH	1.37	0.70	0.81
	$Si(OH)_3$	0.56	1.22	0.51

In Table 5.7[3], the calculated structure data is summarized. The degree of deformation is between 24% and 30%, and the average deformation energy is around 3 eV. As seen previously, $Si(OH)_3$ functional groups deforms the pyrene more than any other functional groups.

Table 5.7 Calculated dihedral angles, degree of deformation (%), and deformation energies (eV) of functionalized pyrene + two metal atoms systems.

C	Metal →	Pt_2			Pd_2			Ni_2		
	Group ↓	Angle	%	D.E.	Angle	%	D.E.	Angle	%	D.E.
D	SiH_3	134.1	25.5	3.26	134.1	25.5	3.26	134.1	25.5	3.26
	NH_2	135.4	24.8	2.77	133.0	26.1	2.65	131.7	26.9	3.33
	OH	128.8	28.4	3.01	129.8	27.9	3.01	129.8	27.9	3.01
A	$Si(OH)_3$	125.3	30.4	3.52	130.2	27.7	3.67	125.7	30.2	3.55
	COOH	135.5	24.7	3.01	136.2	24.3	3.31	131.4	27.0	3.35
	CN	131.1	27.2	3.30	130.9	27.3	3.33	130.5	27.5	3.26

[3]Where C stands for character, D for donor and A for attractor

CHAPTER 6

DISCUSSION OF RESULTS

In this chapter, we will analyze and discuss the results of our calculations. We will first discuss how the selected functionalization groups are anchored on pyrene with the help of the calculated bonding energies and bond orders as a measure of the bond strength. Then, the impact of the functional groups on the deformation of the pyrene will be analyzed. Finally, we will address and discuss the variation of aromaticity of pyrene along the different functionalization paths.

We have shown how metallic particles can be stabilized on functionalized pyrene, and how the metallic particles can induced deformation on the functionalized pyrene molecule. We will attempt to classify the functional groups according to their ability of stabilizing metal particles, supported by the calculated bond orders and bonding energies as criteria.

6.1 Pyrene functionalization

As shown in chapter IV, six different functionalization groups were selected. Three of them are electron donors, while the three other are able to withdraw electronic density. We have selected these functional groups because we wanted to understand how the properties of pyrene (structure, bonding and charge transfer) will be affected by the presence of specific functional groups.

Two kinds of functionalization were considered: homofunctionalization where both functional groups were identical, and heterofunctionalization, where one functional

group plus one hydrogen atom were used.

6.1.1 Bonding energy

We start by sorting the functional groups from the greater to the smaller bonding energy to pyrene:

- Donors: OH > NH_2 > SiH_3
- Attractors: CN > $Si(OH)_3$ > COOH

There are some important observations to address in those results. First, we want to recall that the bonding energies refer to what is called "homolytical breaking" in which both bonds between functional groups and pyrene are simultaneously broken. For heterofunctionalized pyrene, bonding energy represents the amount of energy needed to break the bonds formed between pyrene and the functional group, but also to break pyrene-H bond. A more intensive study of the reaction pathway should be performed to evaluate more accurate the dissociation energy on individual bonds. Nevertheless, as a first approximation, the calculated energies are good indicators of the relative stability of the complexes.

We observed that smaller groups tend to better anchor to pyrene (see table 4.1), therefore they have greater bonding energies and larger bond orders. This could be explained by the fact that smaller functional groups have more localized electrons nearby the atom that is directly bonded to pyrene, therefore strong bonds can be formed. In contrast, electrons can be more delocalized over the whole component of the voluminous groups, and therefore they are forming weaker bonds.

Homo and heterofunctionalization show a similar trend in terms of bond strength, regardless that the second functional group is an hydrogen atom in the heterofunctionalized scheme. This confirms the calculated bond strength trend of the selected groups, since only one group is present and yet the trend is identical.

Donor groups in the heterofunctionalization have higher bonding energies than their counterparts on the heterofunctionalization. This difference in energy could be related to the fact that the carbon atom (C4) in pyrene where hydrogen is bonded is more negatively charged due to its higher electronegativity. Part of this improved electron density can be delocalized near carbon 8 (where the functional group is bonded) and makes the bond C8-functional group stronger.

Finally, we want to mention that as expected, the calculated bonding energy of *trans* complex is higher than the chemical equivalent *cis* complexes. In *trans* complexes, functional groups are at opposite sides of the molecular plane of pyrene, such arrangement decreases the steric effects between functional groups, and therefore compensate and decrease the structural deformation of pyrene.

6.1.2 Bond order

In terms of bond order, we can classify the functional groups from greater to smaller calculated value:

- Donors: $NH_2 \geq OH > SiH_3$
- Attractors: $CN \geq COOH > Si(OH)_3$

As seen in Chapter IV, bond order could be interpreted as the bond strength between atoms in a molecule. Let us first consider the bond order between C8 and

H in the heterofunctionalization. As expected, this value it is between 0.8 - 0.9 (see table 4.8) which, according to the Wiberg theory, represents a single bond. We also want to emphasize on the fact that after the functionalization, every carbon-carbon bonds in pyrene (except for bonds associated to C8 and C4) remained at a value of 1.4 (see Fig 4.11). This means that the aromatic character of the bonds is not totally altered by the functionalization. This is important since the electron delocalization continues to be partly present out of the functionalized region. If some electron density is transferred to pyrene, then this density could be probably delocalized over the π orbitals of the carbon atoms of pyrene.

Also, we have summarized our results of bond orders for homo and heterofunctionalized in tables 4.4 and 4.8 respectively. We see that the smaller groups of every series (OH and CN) as well as the "medium" sized (NH_2, COOH) show bond orders that reflect a single bond with the pyrene molecule. For the $Si(OH)_3$ and SiH_3 groups, we observe bond orders of 0.6 and 0.7, respectively. This is interpreted as a weak bond between the functional group and pyrene, that could be explained by the inductive and steric effects present in these groups.

Si atom in SiH_3 will have a negative formal charge, this could make the bond between carbon and the whole functional group weaker. The opposite behavior is present in $Si(OH)_3$ where oxygen atoms will polarize the bond in the opposite direction, creating a formal positive charge on Si that, in principle, will make the bond stronger, but (as we will see below) the presence of strong steric effects could make the bond weaker.

The polarizability of the functional group may have a significant influence on the magnitude of the bond order obtained. Polarizability is the tendency of a charge distribution to get distorted from its normal shape by the presence of a nearby charge. This can certainly favor an electronic cloud to be displaced towards an

atom with a higher electronegativity, and therefore increasing the strength of the chemical bond. In our case, the NH_2 and OH groups are highly polarizable (Pine, 1980) due to the difference in electronegativity between their atomic components.

In contrast, the steric effect could weaken bonds. As less physical area is available some atoms (or groups of atoms) are "forced" away from their bonding area. In our case, this behavior is present for the "bulkier" $Si(OH)_3$ and SiH_3 groups, and therefore they have smaller bond orders.

6.1.3 Charge transfer

The functionalization groups were finally classified by the magnitude of a net charge transfer:

- Donors: $NH_2 \geq OH > SiH_3$
- Attractors: $Si(OH)_3 > COOH \geq CN$

For the donors functional groups, we see that the order is the same as the one shown for bond order *i.e.* the higher the bond order index is, the higher is the amount of charge transferred from the functional group to C4 and C8 atoms of the pyrene molecule. In contrast, it is the reverse order for the attractor series as shown in Tables 4.3 and 4.7. This last trend is observed for both homo and heterofunctionalization.

The functional group NH_2 has a lone pair of electrons that can be transferred to carbon in pyrene that resulted from a difference of electronegativity between N and C. Bonds involving N and H are polarized for the same reason. An analogue analysis can be done for the OH group. Nevertheless, the flow of charges occurs

in the opposite direction, since the electronegativity of oxygen is higher than for carbon.

The magnitude of the charge transfers can be observed using graphical molecular electrostatical potential surfaces. They correlate with a dipole moment, molecular electronegativity, and partial charges. This type of surface provide a visual method to understand the calculated relative polarity of a molecule. The scale for these graphical representation was chosen to clearly show the change in electrostatic potential. The range of -0.01 to 0.01 is an arbitrary range that emphasizes the zone of variation. The molecular electrostatic potential can be viewed as the potential energy feels by a proton at a particular location near a molecule. Negative electrostatic potential corresponds to the concentrated electron density in the molecules (from lone pairs, pi-bonds, etc.) colored in shades of red. Positive electrostatic potential corresponds to regions where low electron density exists and the nuclear charge is incompletely shielded colored in shades of blue. (Elmhurst College, 2007)

In Figure 6.1, we show a bottom view of functionalized pyrene while in Figure 6.2, a top view is shown.

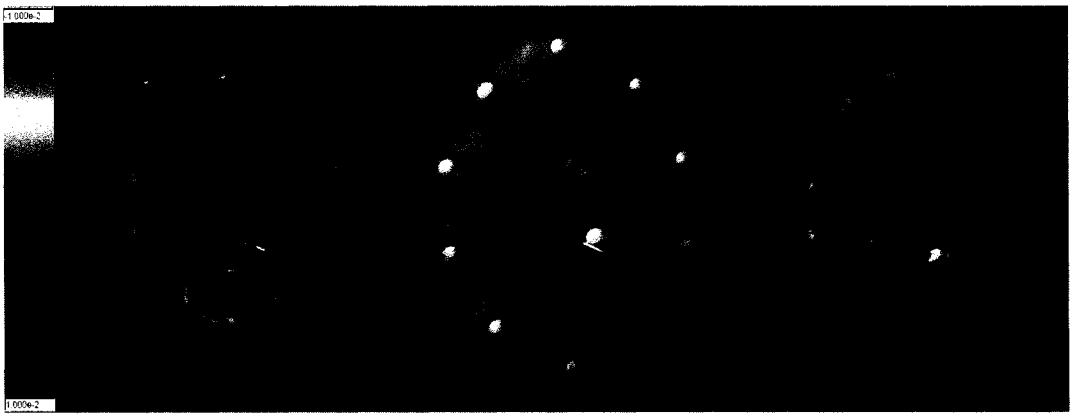

Figure 6.1 Bottom view of an electrostatical potential surface for *cis*-pyrene + donor complexes.

In Figures 6.1 and 6.2, we see an accumulation of electronic density on carbon atoms surrounding the functional groups, while a depletion of it is present in the vicinity of functional groups.

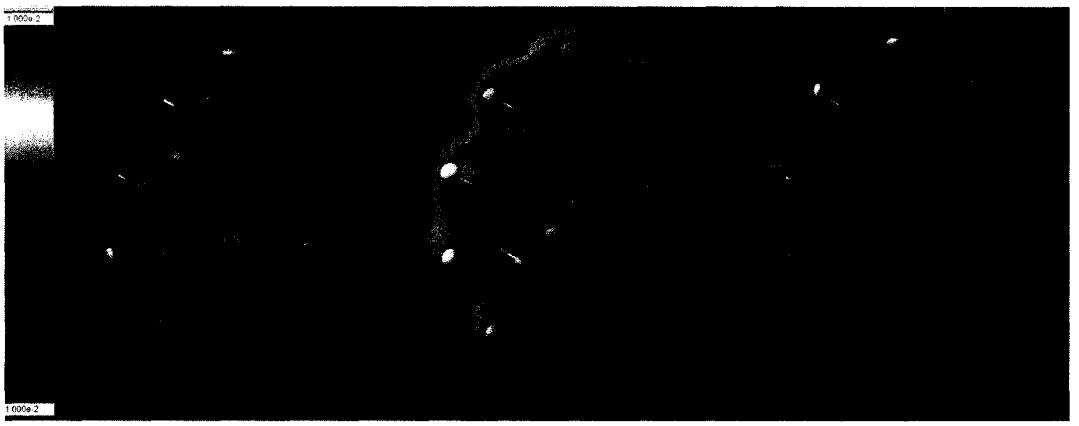

Figure 6.2 Top view of an electrostatical potential surface for *cis*-pyrene + donor complexes.

In figures 6.3 and 6.4, we show the results obtained for the attractor functional groups.

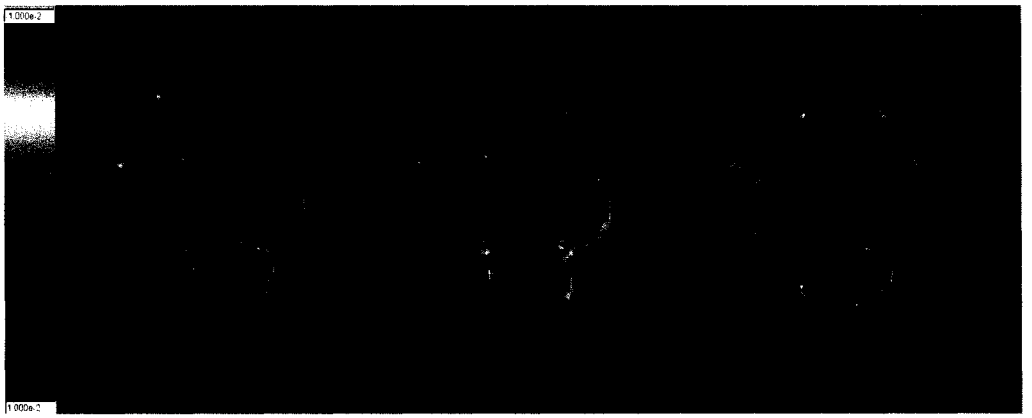

Figure 6.3 Bottom view of an electrostatical potential surface for *cis*-pyrene + attractors complexes.

In contrast to donors, the bonding of attractor groups to pyrene appears to increase the electron density on functional groups, and finally leave a net positive charge on

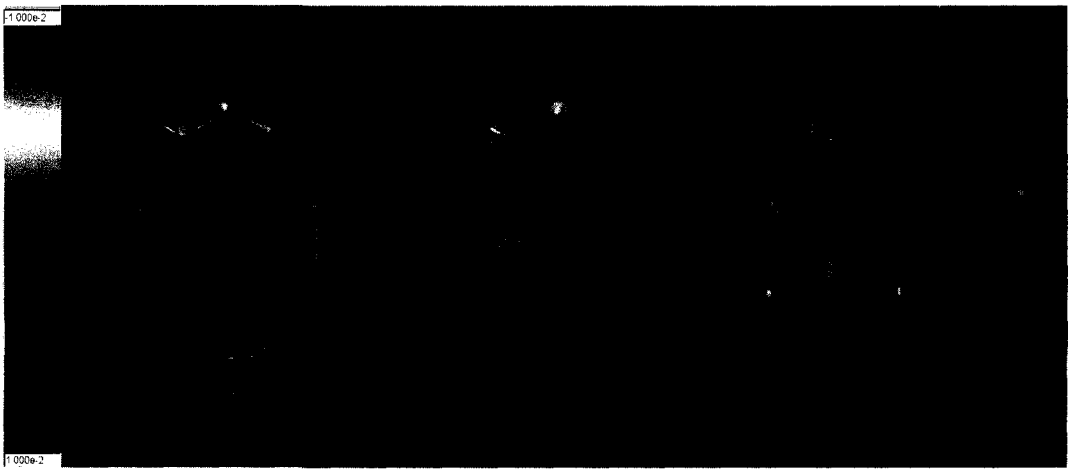

Figure 6.4 Top view of an electrostatical potential surface for *cis*-pyrene + attractor complexes.

pyrene. In *cis*-pyreneCN, a significant electron density transfer occurs from pyrene to the functional group. For $Si(OH)_3$, the electron density is mostly located on pyrene. A similar representation can be drawn for the *trans* complexes, and give similar behavior.

For heterofunctionalization cases, we have noted from Table 4.7 that the carbon atom bonded to functional group (C8) in pyrene gained a net negative charge with donor groups. This result was expected because carbon is more electronegative than hydrogen. Nevertheless, the other carbon atom bonded to the functional group (C4) does not receive any extra negative charge from the donor groups. The presence of hydrogen as functional group reversed the accumulation of electron density to a point where positive charges are obtained on the C4 atom of pyrene. This can be understood since the H atom is a strong donor, a charge transfer occurs to the C8 atom that facilitates a delocalization of the overall charge to the vicinal carbon atoms. Once C4 atom acquires a higher electronic density, the donation effect is reversed.

6.1.4 Structural data

Finally, we analyze the impact of the functionalization on the structural properties of pyrene. We may classify the functional groups on the basis of ability to deform the pyrene molecule in the *cis* homofunctionalization scheme.

- Donors: $NH_2 > SiH_3 > OH$
- Attractors: $Si(OH)_3 > CN > COOH$

We have summarized the calculated structural data for both donor and attractor groups in table 4.2. We observe that *cis* complexes have the greater deformations. This is an expected result since *trans* complexes have the functional groups at opposite sides of pyrene, so that, the deformation exerted by each one of the functional groups will compensate each other, resulting in lower values for the corresponding deformation energies. In contrast, *cis* complexes show deformation values between 25 to 29%. Due to the steric effects, the functional groups tend to separate from each other in a *cis* configuration. As a result of this spatial arrangement, pyrene is strongly deformed, and bends. Another factor that contributes to the deformation of pyrene is the change of hybridization of the central carbon atoms. After the functionalization takes place, carbon atoms go from sp^2 to sp^3 hybridization in order to bond with the functional group. This change of hybridization also occurs in the *trans* complexes, but as it was mentioned this deformation is symmetrical. These effects contribute to the deformation of pyrene which are translated into important values of deformation energy.

If we compare the magnitude of deformation between homo and heterofunctionalization, we observe that most *cis* complexes give similar deformations, but the deformations for the *trans* heterofunctionalizations are greater than homofunction-

alization. This difference for *trans* complexes is due to the fact that deformations exerted by hydrogen is not equally compensate with the functional group in the contrary plane of pyrene.

6.2 Stabilization of metal particles

As showed in chapter V, we have considered the bonding of one and two metal atoms to the functional groups anchored on pyrene. It is important to mention that only *cis* complexes are considered here, since they represent the real model for an external sidewall functionalization of carbon nanotube.

6.2.1 One metal atom particle

First, we consider the bonding of a single metal atom directly to C4 and C8 carbon atoms of pyrene, a "bridge" configuration (see figure 5.1). The different calculated properties are summarized in Table 5.1. We may see that bonding energies for singlet states of the metals considered are low for a chemical adsorption. These low values, in addition to the small bond order calculated between the metal atom and the C4 and C8 carbon atoms, are indicative of a relatively weak bond of the metal to pyrene.

We mentioned in Chapter I, that the coalescence of metal particles increases rapidly when the operation temperature in fuel cells raises. Since metal particles are weakly bonded to the support an increasing temperature will induce the migration and the attachment of this particle to other particles in the surroundings, on which metal-metal bond is favored over metal-support bond.

It is important to mention that the bond order close to 1 observed for Pt and Ni

to pyrene, is a consequence of the significant overlap between the metal orbitals and orbitals of carbon atoms. We also observed that the metal particle adsorption induces a very small deformation of pyrene, which remains almost flat.

Second, we consider the bonding of a single atom metal particle to different *cis* functional groups. The results were summarized in Table 5.2. We immediately see that bonding energies of the metal atom on functional groups are higher than in the "bridge" configuration. A similar tendency is observed for the bond orders. We can summarize our results according to the following rank of bonding energies:

- Attractors: $Si(OH)_3 > COOH > CN$
- Donors: $NH_2 > SiH_3 > OH$

Attractor groups showed the higher bonding energies and also the higher bond order values. Therefore, they would stabilized the one metal atom particle better than the donors. Nevertheless, NH_2 has 1.91 eV value for bonding energy and a bond order of almost one with respect to Pt. Among the selected functional groups, the three attractors and at least one donor (NH_2) seem to be promising candidates to be considered as choices for an experimental functionalization.

Regarding the charge transfer, we observed that attractors leave the metal atoms positively charged while for the donors, the transfer of the charge is negligible. With the type of charge analysis we have performed, it remains very difficult to say without doubts that the withdrawn charge from the metal atoms become delocalized over the entire pyrene. Further calculations on larger models are required to better answer this particular issue.

If we compare the stabilization of the metal particle with and without the presence of a functional group, the result of our calculations strongly suggest that functional

groups may play an important role in the metallic stabilization. The fact of having greater bonding energies, and greater bond orders allow us to undeniably arrive to the conclusion that, metallic particles are more stable when bonded to pyrene that has been functionalized. Nevertheless, we can not say if the presence of functional group will affect the reactivity of Pt particles for fuel cell applications.

6.2.2 Two metal atom particles

The stabilization of two metal atoms particles (see figure 5.3) gives the same ranking for the bonding energies and the calculated bond orders, than for the single atoms particles.

- Attractors: $Si(OH)_3 > COOH > CN$
- Donors: $NH_2 > SiH_3 > OH$

We have obtained the same tendency for the two metal atom particles as we expected, since we have the same bonding scheme of one atom interacting with the functional group. The values of bonding energies are of the same magnitude, comparable with the one metal particle results.

Bond order analysis is summarized in table 5.6, where NH_2 and SiH_3 groups display bond orders of two for Pt and Pd. The OH group has the weakest bond order of the whole series. A possible explanation is that OH forms a strong bond with carbon atom in pyrene, its donor character induces a depletion of the electron density towards pyrene, that ultimately weakens its bonding with the metal atom.

For the attractors, the $Si(OH)_3$ group has the highest value of bonding energy and bond order for Pt. Although CN is strongly bonded to pyrene, it has a weak

stabilizing effect on the metal particles. In contrast, the $Si(OH)_3$ group forms strong bond with metal particles. This could be explained, by the high electron density that surrounds Si atom, and by the important overlapping between orbitals of Si and metal atoms.

Structural data shows deformations of pyrene that are comparable with those obtained for one metal atom stabilization. The presence of the metal particles does not change significantly the structure of pyrene. This is an important result since greater deformations or the breaking of vicinal bonds can alter the electron transport within the $\pi - \pi$ conjugation systems.

CONCLUSIONS

After analyzing our results, we arrive to the following conclusions:

- For the chosen series of donor and attractor groups, the attractor groups (CN, $Si(OH)_3$, COOH) have greater bonding energies and higher bond orders than the donor groups (OH, NH_2, SiH_3) for both homo and heterofunctionalization schemes.
- Homofunctionalization and heterofunctionalization showed the same tendency in terms of bond "strength" to pyrene.
- If a metal particle is adsorbed on pyrene with functional groups, the bonding energies and the bond orders are higher than when no functional groups are present. Therefore, the metal particles are more stabilized on functionalized pyrene. Although we believe this should decrease the magnitude of coalescence, we can not comment on the resulting reactivity of the metal particles.
- Once the metal particles are stabilized on pyrene, the electron density tends to accumulate on pyrene. This suggest that once molecular hydrogen is split (during fuel cell anodic reaction) the resulting electrons could also be more easily transferred to the support.
- We found that Nickel has the smallest calculated values of bonding energies and bond orders (among the selected functional groups), while Pt showed the highest values for the chosen metal particles.
- The functionalizations deformed importantly the pyrene molecule. The presence of the functional groups makes pyrene to bend. Nevertheless, the $\pi - \pi$ conjugation is mostly preserved among pyrene with more significant variations near the functionalization sites due to a change in hybridization (from

sp^2 to sp^3) of the carbon atoms involved in the bonding with the functional groups.

- The new shape of the functionalized pyrene resembles the curvature of a (10,10) carbon nanotube. In principle, this shows that the functionalization of a carbon nanotube would not have to overcome the energetic barrier of deformation like for pyrene. Therefore, functionalization of CNT should be "easier" to accomplish than pyrene functionalization.

In order to extend this research project, we would suggest to investigate the following points:

- Analyze this results in terms of orbitals, to determine if there is overlapping between functional groups orbitals and orbitals of the carbon atoms in pyrene.
- Study the reaction path of all the performed functionalizations. In order to establish the feasibility of performing these functionalizations experimentally.
- Use a more realistic metallic particle model.
- To model the splitting of H_2 molecule at the surface of the metallic particle. Subsequently to analyze the charge transportation phenomena. This could help to analyze, if some electron density will flow from the metal-hydrogen site, through the functional group to be finally delocalized over the pyrene rings.
- To model CNT, and try to reproduce the tendency that we obtained during the course of the present research. This can be done using SWCNT as a preliminary step to the study. Perform a whole model relaxation, and then the functionalization, using the same functional groups and allowing only the reaction site to be relaxed.

REFERENCES

Andrae, D., Haussermann, U., Dolg, M., Stoll, H., and Preuss, H. (1990). Energy-adjusted ab initio pseudopotentials for the second and third row transition elements. *Theoretica Chimica Acta*, **77**(2), 123–141.

Atkins, P. W. and Friedman, R. S. (1997). *Molecular Quantum Mechanics*, chapter 9, pages 276–319. Oxford University Press, 3^{rd} edition.

Bahr, J., Yang, J., Kosynkin, D., Bronikowski, M., Smalley, R., and Tour, J. (2001). Functionalization of carbon nanotubes by electrochemical reduction of aryl diazonium salts: A bucky paper electrode. *Journal of the American Chemical Society*, **123**(27), 6536–6542.

Becke, A. D. (1988). Density-functional exchange-energy approximation with correct asymptotic behavior. *Phys. Rev. A*, **38**(6), 3098–3100.

Becke, A. D. (1992a). Density-functional thermochemistry. i. the effect of the exchange-only gradient correction. *Journal of Chemical Physics*, **96**(3), 2155.

Becke, A. D. (1992b). Density-functional thermochemistry. iii. the effect of the perdew-wang generalized-gradient correlation correction. *Journal of Chemical Physics*, **97**(12), 9173.

Becke, A. D. (1993). Density-functional thermochemistry. iii. the role of exact exchange. *Journal of Chemical Physics*, **98**(7), 5648.

Becke, A. D. (1996). Density-functional thermochemistry. iv. a new dynamical correlation functional and implications for exact-exchange mixing. *Journal of Chemical Physics*, **104**(3), 1040.

Becke, A. D. (1997). Density-functional thermochemistry. v. systematic optimization of exchange-correlation functionals. *Journal of Chemical Physics*, **107**(20), 8554.

Bergner, A., Dolg, M., Kuchle, W., Stoll, H., and Preuss, H. (1993). Ab initio energy-adjusted pseudopotentials for elements of groups 13-17. *Molecular Physics*, **80**(6), 1431–1441.

Born, M. and Oppenheimer, J. (1927). On the quantum theory of molecules. *Ann. Physik*, **84**, 457.

Chen, E. (2003). *Fuel Cells Technology Handbook*, chapter History, pages 2–1 to 2–40. CRC Press, 1^{st} edition.

Chen, R., Zhang, Y., Wang, D., and Dai, H. (2001). Noncovalent sidewall functionalization of single-walled carbon nanotubes for protein immobilization. *Journal of the American Chemical Society*, **123**(16), 3838–3839.

Dolg, M., Wedig, U., Stoll, H., and Preuss, H. (1987). Energy-adjusted ab initio pseudopotentials for the first row transition elements. *Journal of Chemical Physics*, **86**(2), 866–872.

Dresselhaus, M. S., Dresselhaus, G., and Saito, R. (1992). Carbon fibers based on C_{60} and their symmetry. *Phys. Rev. B*, **45**(11), 6234–6242.

Elmhurst College (2007). Virtual ChemBook. from: http://www.elmhurst.edu/$\sim$chm/vchembook/211elecpotential.html, Consulted February 22^{nd} 2008.

Figgen, D., Rauhut, G., Dolg, M., and Stoll, H. (2005). Energy-consistent pseudopotentials for group 11 and 12 atoms: adjustment to multi-configuration dirac-hartree-fock data. *Chemical Physics*, **311**(1-2), 227–244.

Foresman, J. and Frisch, A. (1996a). *Exploring Chemistry with Electronic Structure Methods*, chapter 2-4, pages 13–90. Gaussian Inc., 2^{nd} edition.

Foresman, J. and Frisch, A. (1996b). *Exploring Chemistry with Electronic Structure Methods*, chapter Single Point Energy Calculation, pages 13–37. Gaussian Inc., 2^{nd} edition.

Frisch, J., Trucks, G., Schlegel, H., Scuseria, E., Robb, M., Cheeseman, J., Montgomery, J., Vreven, T., Kudin, K., Burant, J., Millam, J., Iyengar, S., Tomasi, J., Barone, V., Mennucci, B., Cossi, M., Scalmani, G., Rega, N., Petersson, G., Nakatsuji, H., Hada, M., Ehara, M., Toyota, K., Fukuda, R., Hasegawa, J., Ishida, M., Nakajima, T., Honda, Y., Kitao, O., Nakai, H., Klene, M., Li, X., Knox, J., Hratchian, H., Cross, J., Adamo, C., Jaramillo, J., Gomperts, R., Stratmann, R., Yazyev, O., Austin, A., Cammi, R., Pomelli, C., Ochterski, J., Ayala, P. Morokuma, K., Voth, G., Salvador, P., Dannenberg, J., Zakrzewski, V., Dapprich, S., Daniels, A., Strain, M., Farkas, O., Malick, D., Rabuck, A., Raghavachari, K., Foresman, J., Ortiz, J., Cui, Q., Baboul, A., Clifford, S., Cioslowski, J., Stefanov, B., Liu, G., Liashenko, A., Piskorz, P., Komaromi, I., Martin, R., Fox, D., Keith, T., Al-Laham, M., Peng, C., Nanayakkara, A., Challacombe, M., Gill, P., Johnson, B., Chen, W., Wong, M., Gonzalez, C., and Pople, J. (2004). *Gaussian 03, Revision C.02.* Gaussian Inc.

Fuentealba, P., Stoll, H., von Szentpaly, L., Schwerdtfeger, P., and Preuss, H. (1983). On the reliability of semi-empirical pseudopotentials: simulation of hartree-fock and dirac-fock results. *Journal of Physics B (Atomic and Molecular Physics)*, **16**(11), 323–328.

GeneralMotors (2006). GM heritage center shares history of hydrogen fuel cells. from: http://www.gm.com/company/gmability/adv_tech/100_news, Consulted February 22^{nd} 2007.

Grove, W. (1839). On voltaic series and the combination of gases and platinum. *Philosophical Magazine and Journal of Science*, **3**(14), 127–130.

Hamada, N., Sawada, S., and Oshiyama, A. (1992). New one-dimensional conductors: Graphitic microtubules. *Phys. Rev. Lett.*, **68**(10), 1579–1581.

Hamon, M., Hu, H., Bhowmik, P., Niyogi, S., Zhao, B., Itkis, M., and Haddon, R. (2001). End-group and defect analysis of soluble single-walled carbon nanotubes. *Chemical Physics Letters*, **347**, 8–12.

Hernandéz, J., García, I., and Martínez, J. (2004). Topological analysis of the electron density and of the electron localization function of pyrene and its radicals. *Chem. Phys.*, (308), 181–192.

Hirsch, A. (2002). Functionalization of single-walled carbon nanotubes. *Angewandte Chemie International Edition*, **41**(11), 1853–1859.

Hohenberg, P. and Kohn, W. (1964). Inhomogeneous electron gas. *Phys. Rev.*, **136**(3B), B864–B871.

Holzinger, M., Vostrowsky, O., Hirsch, A., Hennrich, F., Kappes, M., Weiss, R., and Jellen, F. (2001). Sidewall functionalization of carbon nanotubes. *Angewandte Chemie International Edition*, **40**(21), 4002–4005.

Hoogers, G. (2003a). *Fuel Cells Technology Handbook*, chapter Introduction, pages 1–1 to 1–5. CRC Press, 1^{st} edition.

Hoogers, G. (2003b). *Fuel Cells Technology Handbook*, chapter The Fueling Problem: Fuel Cells Systems, pages 5–1 to 5–23. CRC Press, 1^{st} edition.

Igel, G., Stoll, H., and Preuss, H. (1988). Pseudopotentials for main group elements (iiia through viia). *Molecular Physics*, **65**(6), 1321–1328.

Kohn, W. and Sham, L. J. (1965). Self-consistent equations including exchange and correlation effects. *Phys. Rev.*, **140**(4A), A1133–A1138.

Krishnan, R., Binkley, J., Seeger, R., and Pople, J. (1980). Self-consisted molecular orbital methods. XX. A basis set for a correlated wave functions. *Journal of Chemical Physics*, **72**(1), 650–654.

Krstic, V., Duesberg, G., Muster, J., Burghard, M., and Roth, S. (1998). Langmuir-blodgett films of matrix-diluted single-walled carbon nanotubes. *Chemistry of Materials*, **10**(9), 2338–2340.

Lee, C., Yang, W., and Parr, R. G. (1988). Development of the colle-salvetti correlation-energy formula into a functional of the electron density. *Phys. Rev. B*, **37**(2), 785–789.

Levine, I. (1999a). *Quantum Chemistry*, chapter Comparisons of Methods, pages 693–709. Prentice Hall, 5^{th} edition.

Levine, I. (1999b). *Quantum Chemistry*, chapter $Ab-Initio$ and DFT treatments of molecules, pages 480–625. Prentice Hall, 5^{th} edition.

Li, H., Lu, W., Li, J., Bai, X., and Gu, C. (2005). Multichannel ballistic transport in multiwall carbon nanotubes. *Physical Review Letters*, **95**(8), 086601–086605.

Lim, I., Schwerdtfeger, P., Metz, B., and Stoll, H. (2005). All-electron and relativistic pseudopotential studies for the group 1 element polarizabilities from k to element 119. *Journal of Chemical Physics*, **122**(10), 104–103.

McEuen, P., Bockrath, M., Cobden, D., Yoon, Y., and Louie, S. (1999). Disorder, pseudospins, and backscattering in carbon nanotubes. *Phys. Rev. Lett.*, **83**(24), 5098–5101.

Mickelson, E., Huffman, C., Rinzler, A., Smalley, R., Hauge, R., and argrave, J. (1998). Fluorination of single-wall carbon nanotubes. *Journal of Physics: Condensed Matter*, **296**, 188 – 194.

Mintmire, J., Dunlap, B., and White, C. (1992). Are fullerene tubules metallic? *Phys. Rev. Lett.*, **68**(5), 631–634.

Moffitt, W. and Coulson, C. (1948). The elctronic structure and bond lengths of coronene and pyrene. *Proc. Phy. Soc.*, **60**(340), 309–315.

Neugebauer, J., Baerends, E., Efremov, E., Ariese, F., and Gooijer, C. (2005). Combined theoretical and experimental deep-uv resonance raman studies of substituted pyrenes. *Journal of Physical Chemistry A*, **109**(10), 2100 – 2106.

Okazaki, T., Suenaga, K., Hirahara, K., Bandow, S., Iijima, S., and Shinohara, H. (2001). Real time reaction dynamics in carbon nanotubes. *Journal of the American Chemical Society*, **123**(39), 9673–9674.

Park, Y. and Cheong, B. (2006). Theoretical investigation of electronic structures of the ground and excited states of pyrene and its derivatives. *Current Applied Physics*, **6**(4), 700 – 705.

Peng, C., Ayala, P. Y., Schlegel, H. B., and Frisch, M. J. (1996). Using redundant internal coordinates to optimize equilibrium geometries and transition states. *Journal of Computational Chemistry*, **17**(1), 49 – 56.

Peuckert, M., Yoneda, T., Betta, R. A. D., and Boudart, M. (1986). Oxygen reduction on small supported platinum particles. *Journal of The Electrochemical Society*, **133**(5), 944–947.

Pine, S. H. (1980). *Organic Chemistry*, chapter Structure, Reactivity, And Organic Transformations, pages 196–239. Mc. Graw Hill, 4^{th} edition.

Rao, R., Satishkumar, B. Govindaraj, A., and Nath, M. (2001). Nanotubes. *ChemPhysChem*, **2**(2), 78–105.

Rideal, E. K. and Evans, U. (1922). The problem of the fuel cell. *Transactions of the Farday Society*, **17**, 466–482.

Robertson, J. and White, J. (1945). The crystal structure of pyrene. a quantitative x-ray investigation. *J. Chem. Soc., ibid*(607), 358–361.

Saito, R. (1998). *Physical Properties of Carbon Nanotubes*, chapter Structure of a Single-Wall Carbon Nanotube, pages 35–38. Imperial College Press, 1^{st} edition.

Salvetat, J.-P., Bonard, J.-M., Thomson, N., Kulik, A., Forro, L., Benoit, W., and Zuppiroli, L. (1999). Mechanical properties of carbon nanotubes. *Applied Physics A: Materials Science and Processing*, **69**(3), 255 – 260.

Smith, B., Monthioux, M., and Luzzi, D. (1999). Carbon nanotube encapsulated fullerenes: a unique class of hybrid materials. *Chemical Physics Letters*, **315**, 31–36.

Star, A., Fraser, J., Steuerman, D., Diehl, M., Boukai, A., Wong, E., Yang, X., Chung, S., Choi, H., and Heath, J. (2001). Preparation and properties of polymer-wrapped single-walled carbon nanotubes. *Angewandte Chemie International Edition*, **40**(9), 1721–1725.

Sun, X., Li, R., Stansfield, B., Dodelet, J., and Desilets, S. (2004). 3d carbon nanotube network based on a hierarchical structure grown on carbon paper backing. *Chemical Physics Letters*, **394**, 266–270.

Szabo, A. and Ostlund, N. (1996a). *Introduction to Advanced Electronic Structure Theory*, chapter 2, pages 39–107. Dover, 1^{st} edition.

Szabo, A. and Ostlund, N. (1996b). *Introduction to Advanced Electronic Structure Theory*, chapter 3, pages 108–230. Dover, 1^{st} edition.

Uchida, M., Fukuoka, Y., Sugawara, Y., Eda, N., and Ohta, A. (1996). Effects of microstructure of carbon support in the catalyst layer on the performance of polymer-electrolyte fuel cells. *Journal of The Electrochemical Society*, **143**(7), 2245–2252.

Villers, D., Sun, S., Serventi, A., Dodelet, J., and Desilets, S. (2006). Characterization of pt nanoparticles deposited onto carbon nanotubes grown on carbon paper and evaluation of this electrode for the reduction of oxygen. *Journal of Physical Chemistry B*, **110**(51), 25916–25925.

Wade, L.G., J. (1999). *Organic Chemistry*, chapter Conjugated Systems, Orbital Symmetry and Ultraviolet Spectroscopy, pages 647–689. Prentice Hall, 4^{th} edition.

Wang, C., Waje, M., Wang, X., Tang, J., Haddon, R., and Yan, Y. (2004). Proton exchange membrane fuel cells with carbon nanotube based electrodes. *Nano Letters*, **4**(2), 345–348.

White, C., Robertson, D., and Mintmire, J. (1993). Helical and rotational symmetries of nanoscale graphitic tubules. *Phys. Rev. B*, **47**(9), 5485–5488.

Wiberg, K. (1968). Application of the pople-santry-segal cndo method to the cyclopropylcarbinyl and cyclobutyl cation and to bicyclobutane. *Tetrahedron*, **24**, 1083–1096.

Wilson, M. and Madden, P. (2001). Growth of ionic crystals in carbon nanotubes. *Journal of the American Chemical Society*, **123**(9), 2101–2102.